

# Predictive Scaling Laws for Spherical Rotating Dynamos

L. Oruba and E. Dormy

## Abstract

State of the art numerical models of the Geodynamo are still performed in a parameter regime extremely remote from the values relevant to the physics of the Earth's core. In order to establish a connection between dynamo modeling and the geophysical motivation, it is necessary to use scaling laws. Such scaling laws establish the dependence of essential quantities (such as the magnetic field strength) on measured or controlled quantities. They allow for a direct confrontation of advanced models with geophysical constraints.

We combine a numerical approach, based on a multiple linear regression method in the form of power laws, applied to a database of 102 direct numerical simulations (courtesy of U. Christensen), and a physical approach, based on energetics and forces balances.

We show that previous empirical scaling laws for the magnetic field strength essentially reflect the statistical balance between energy production and dissipation for saturated dynamos. Such power based scaling laws are thus necessarily valid for any dynamo in statistical equilibrium and applicable to any numerical model, irrespectively of the dynamo mechanism.

We show that direct numerical fits can provide contradictory results owing to biases in the parameters space covered in the numerics and to the role of a priori hypothesis on the fraction of ohmic dissipation.

We introduce predictive scaling laws, i.e. relations involving input parameters of the governing equations only. We guide our reasoning on physical considerations. We show that our predictive scaling laws can properly describe the numerical database and reflect the dominant forces balance at work in these numerical simulations. We highlight the dependence of the magnetic field strength on the rotation rate. Finally, our results stress that available numerical models operate in a viscous dynamical regime, which is not relevant to the Earth's core.

## 1 Introduction

Many numerical models have been produced over the last few years to try and reproduce characteristics of planetary and stellar magnetic fields. The parameter regime relevant to these natural objects is however out of reach of present days computational resources. In order to assess the reliability of current numerical models and their relevance to natural applications, it is thus necessary to rely on scaling laws, which can be established on the basis of a set of numerical models with varying control parameters and then extended to the regime of geophysical or astrophysical relevance.

Previous empirical scaling laws for the magnetic field strength (Christensen & Aubert, 2006) have proven to be remarkably robust. Indeed they seem to be applicable to numerical models irrespectively of the parameter regime, viscous or inertial (Christensen, 2010; Schinnerer et al., 2012), as well as to natural objects of very different kinds (Christensen et al., 2009). Such scaling laws are constructed on the basis of a statistical balance between energy production and dissipation. It is essential to separate the relative importance of this general assumption –which will necessarily be valid for any dynamo in statistical equilibrium– from additional assumptions which could test the nature of a particular dynamo. An additional key issue is that such existing relations only relate measured quantity. They

have no predictive power for numerical models in the sense that the knowledge of control parameters (entering the governing equations) is not sufficient to a priori estimate the strength of the produced magnetic field. We therefore want to introduce predictive scaling laws, which a priori estimate the amplitude of a measured quantity (say the magnetic field strength) as a function of input parameters only.

## 2 Governing equations and numerical models

We restrict our study to Boussinesq models of planetary dynamos. The domain consists of a spherical shell, and the aspect ratio between the two bounding spheres is set to  $\xi \equiv r_i/r_o = 0.35$ . The flow is driven by an imposed difference of temperature between the inner and outer boundaries.

The governing equations in the rotating reference frame can then be written – using  $L = r_o - r_i$  as unit of length,  $\Omega^{-1}$  as unit of time,  $\Delta T$  as unit of temperature, and  $\sqrt{\rho\mu}\Omega L$  as unit for the magnetic field – as

$$\partial_t \mathbf{u}^* + (\mathbf{u}^* \cdot \nabla) \mathbf{u}^* = -\nabla \pi^* + E \Delta \mathbf{u}^* - 2\mathbf{e}_z \times \mathbf{u}^* + \frac{\text{Ra} E^2}{\text{Pr}} T^* \frac{\mathbf{r}}{r_o} + (\nabla \times \mathbf{B}^*) \times \mathbf{B}^*, \quad (1)$$

$$\partial_t \mathbf{B}^* = \nabla \times (\mathbf{u}^* \times \mathbf{B}^*) + \frac{E}{\text{Pm}} \Delta \mathbf{B}^*, \quad \partial_t T^* + (\mathbf{u}^* \cdot \nabla) T^* = \frac{E}{\text{Pr}} \Delta T^*, \quad (2)$$

$$\nabla \cdot \mathbf{u}^* = \nabla \cdot \mathbf{B}^* = 0. \quad (3)$$

Because the governing equations involve nine independent physical parameters ( $\alpha$ ,  $g_0$ ,  $\Delta T$ ,  $\nu$ ,  $\kappa$ ,  $\eta$ ,  $\Omega$ ,  $\rho$ ,  $\mu$ ) and five units (kg, m, s, K, C), owing to the Buckingham  $\pi$  theorem, only four independent non-dimensional parameters can be introduced. In our system (1–3), they are the Ekman number  $E = \nu/(\Omega L^2)$ , the Prandtl number  $\text{Pr} = \nu/\kappa$ , the magnetic Prandtl number  $\text{Pm} = \nu/\eta$ , and the Rayleigh number  $\text{Ra} = \alpha g_0 \Delta T L^3/(\nu \kappa)$ , in which  $\nu$  is the kinematic viscosity of the fluid,  $\alpha$  the coefficient of thermal expansion,  $g_0$  the gravity at the outer bounding sphere,  $\kappa = k/(\rho c)$  its thermal diffusivity, and  $\eta$  its magnetic diffusivity. Throughout this article, non-dimensional quantities are denoted with a  $*$ .

All the simulations used in this work rely on no-slip mechanical boundary conditions and an insulating outer domain. The inner core is insulating in most simulations, and a few simulations involve a conducting inner core with the same conductivity as the fluid.

Our analysis will be tested against a wide database of 185 direct numerical simulations kindly provided by U. Christensen. The data sample is reduced to 102 to only take into account dynamo simulations corresponding to fully developed convection ( $\text{Nu} > 2$ ) and producing a dipolar magnetic field (relative dipole field strength  $f_{\text{dip}}$  larger than 0.5). Moreover, we limit our study to  $\text{Pr} \leq 10$ , that is to say to values not too far from the value estimated for the Earth’s core. We will also highlight the subset of this database which was used in Christensen & Aubert (2006). It is composed of 65 runs available at the time. Finally we will use a few additional numerical data published in Morin & Dormy (2009).

These numerical data can be used to test scaling laws guided by physical reasoning. It can also be used to establish direct numerical fits. To this end, we introduce a multiple linear regression approach (Montgomery et al., 2001; Cornillon & Matzner-Lober, 2010), detailed in appendix A.

### 3 Power based scalings, key parameters and their relations

#### 3.1 Energy balance between production and dissipation

In order to derive a scaling law for the magnetic field strength, a possible approach introduced by Christensen & Aubert (2006) is to consider the statistical balance between energy production by buoyancy forces and dissipation. Time averaged quantities of a statistically steady dynamo state should obviously satisfy

$$P = D_\eta + D_\nu, \quad (4)$$

where  $P$  is the power generated by buoyancy forces,  $D_\eta$  is the rate of ohmic dissipation

$$D_\eta = \int_V \frac{\eta}{\mu} (\nabla \times \mathbf{B})^2 dV, \quad \text{i.e.} \quad D_\eta^* = E_\eta \int_V (\nabla \times \mathbf{B}^*)^2 dV^*,$$

in which  $E_\eta = E/Pm$  is the magnetic Ekman number and  $D_\nu$  is the rate of viscous dissipation

$$D_\nu = \int_V \rho \nu (\nabla \times \mathbf{u})^2 dV, \quad \text{i.e.} \quad D_\nu^* = E \int_V (\nabla \times \mathbf{u}^*)^2 dV^*.$$

The above quantities are all defined as time averaged over a sufficient amount of time, so that they are steady for a given parameter set.

Following Christensen & Aubert (2006) and introducing the  $f_{\text{ohm}}$  coefficient, defined as

$$f_{\text{ohm}} \equiv \frac{D_\eta}{D_\eta + D_\nu}, \quad (5)$$

we get

$$P = \frac{D_\eta}{f_{\text{ohm}}} = \frac{1}{f_{\text{ohm}}} \int_V \frac{\eta}{\mu} (\nabla \times \mathbf{B})^2 dV \sim \frac{1}{f_{\text{ohm}}} \frac{\eta}{\mu} \frac{B^2}{\ell_B^2} V, \quad (6)$$

where we introduced a typical magnetic field strength  $B$  and a magnetic dissipation length scale  $\ell_B$ , defined again using time averaged quantities as

$$\ell_B^2 \equiv \frac{\int_V \mathbf{B}^2 dV}{\int_V (\nabla \times \mathbf{B})^2 dV} = 2\eta \frac{E_{\text{mag}}}{D_\eta} \quad \text{i.e.} \quad \ell_B^{*2} \equiv 2E_\eta \frac{E_{\text{mag}}^*}{D_\eta^*}, \quad (7)$$

$$\text{with} \quad E_{\text{mag}} = \int_V \frac{\mathbf{B}^2}{2\mu} dV, \quad \text{i.e.} \quad E_{\text{mag}}^* = \int_V \frac{\mathbf{B}^{*2}}{2} dV^*. \quad (8)$$

This simple reasoning provides the following expression for the magnetic field strength

$$\frac{B^2}{\mu} \sim f_{\text{ohm}} \ell_B^2 \frac{P}{\eta V} = f_{\text{ohm}} \ell_B^2 \frac{\rho P_M}{\eta}, \quad (9)$$

where  $P_M$  is the mass power generated by buoyancy forces  $P_M \equiv P/(\rho V)$ .

The non-dimensional form of equation (9) is

$$Lo \sim f_{\text{ohm}}^{1/2} P^{1/2} E_\eta^{-1/2} \ell_B^*, \quad (10)$$

where  $Lo \equiv (2 E_{\text{mag}}^*/V^*)^{1/2} \equiv B^*$ . Expressing a scaling law for  $B$  (or its non-dimensional form  $Lo$ ) therefore reduces to relating  $P$  and  $\ell_B$  to the relevant parameters.

In previous studies  $\ell_B$  has often not been introduced as such (but see the review by Roberts & King, 2013). Instead it is usually indirectly evaluated by introducing the magnetic dissipation time  $\tau_{\text{diss}} \equiv E_{\text{mag}}/D_\eta = \ell_B^2/(2\eta)$  (see Christensen & Tilgner, 2004), or in non-dimensional form  $\tau_\eta^* \equiv \tau_{\text{diss}}/\tau_{\text{dip}}$ , where  $\tau_{\text{dip}} \equiv L^2/(\pi^2 \eta)$ . This definition leads to  $\tau_\eta^* = \pi^2/2 \ell_B^{*2}$ . Besides, the parameter  $f_{\text{ohm}}$  is a rather complex number, which involves both a priori input and a posteriori output model properties. It is usually assumed to be order one in natural dynamos (but see Schinnerer, 2012), its importance in scaling laws is discussed in appendix B.

### 3.2 Power generated by buoyancy forces

Christensen & Aubert (2006) established a relation between  $P^*$  and a flux-based Rayleigh number  $Ra_Q^*$

$$Ra_Q^* \equiv \frac{1}{4\pi r_o r_i} \frac{\alpha g r_o \Delta Q}{\rho c \Omega^3 (r_o - r_i)^2}, \quad (11)$$

where  $\Delta Q$  is the difference between the time-average total heat flow  $Q$  and  $Q_d^{T_s} = 4\pi k T_a$  ( $J \cdot s^{-1}$ ), which corresponds to the diffusive heat flow associated to  $T_S(r) = T_a/r + T_b$ .

They show that

$$P^* \approx 2\pi \xi \frac{1 + \xi}{(1 - \xi)^2} Ra_Q^*, \quad (12)$$

under the assumptions that the volume integral of the realised temperature gradient can be approximated by its conductive counterpart. The demonstration requires in particular fixed temperature boundary conditions. Relation (12) is well-verified for the numerical database used in the present study. That is why in the following numerical analysis of scaling laws, the parameter  $P^*$  will be replaced by  $Ra_Q^*$  with a prefactor of 7.03 determined by the geometry via the aspect ratio  $\xi$ .

It is important to stress that  $Ra_Q^*$  is an output parameter, and cannot be controlled a priori when using fixed temperature boundary conditions. It can however be related to the classical Rayleigh number, which is a control parameter of the problem. Indeed, introducing the Nusselt number  $Nu \equiv Q/Q_d^{T_s}$ , which can be rewritten as  $Nu = Q_d(r_o)/(4\pi k T_a)$  under the statistically steady assumption, relation (11) becomes

$$Ra_Q^* = E^3 Pr^{-2} Ra (Nu - 1). \quad (13)$$

The  $Ra_Q^*$  parameter can not be controlled in the problem because it is related to the output parameter  $Nu$ . Its value is zero at the onset of convection ( $Nu = 1$ ).

Note that  $Ra_Q^* Nu/(Nu - 1)$  would be an input control parameter in the case of imposed heat flux boundary conditions. The construction of  $Ra_Q^*$  would however still involve, even with such boundary conditions, measurements of the Nusselt number, because the temperature difference across the shell becomes a measured quantity.

### 3.3 Role of the magnetic dissipation length scale $\ell_B$

In the numerical database used in the present paper, the dissipation length scale  $\ell_B^*$ , calculated using equation (7), varies between 0.02 and 0.10. These values are obviously smaller than those corresponding to the pure dipole decay in the absence of motions  $\tau_\eta^* = 1/2$ , i.e.  $\ell_B^* = 1/\pi \simeq 0.30$ . Besides, the range of variation of  $\ell_B^*$  is less than one order of magnitude. Thus, as a first approximation, the variations of  $\ell_B^*$  can be neglected, namely it can be set to a constant in equation (10). Using the relation (12), equation (10) becomes under this assumption

$$Lo \sim f_{ohm}^{1/2} Ra_Q^{*1/2} E_\eta^{-1/2}. \quad (14)$$

Its application to the 102 dynamos database is represented in figure 1, and yields the relative misfit  $\chi_{rel} = 0.433$ . Relation (14), which simply corresponds to the energy balance between production and dissipation with  $\ell_B$  approximated as a constant, already provides a good fit to the numerical data. This implies that empirical fits of the magnetic field strength previously obtained in the literature mainly reflect this simple balance between energy production and dissipation, combined with an improved description of the magnetic dissipation  $\ell_B$  than a simple constant, which is however not essential.

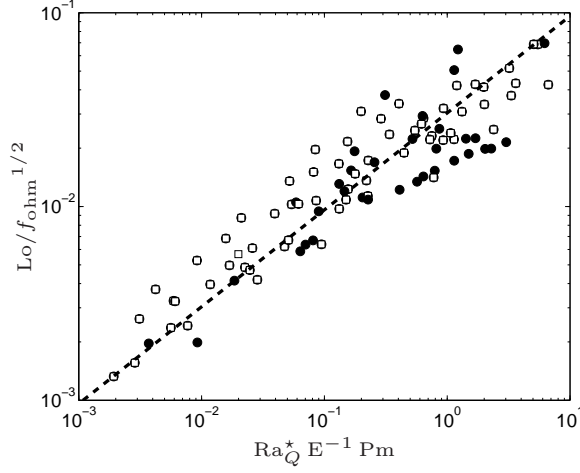


Figure 1: The Lorentz number corrected for the relative fraction of Ohmic dissipation versus a combination of the flux-based Rayleigh number, the Ekman number and the magnetic Prandtl number: equation (14). This simple scaling law only reflects the statistical balance between energy production and dissipation, combined with a constant  $\ell_B$ . Points correspond to the full 102 dynamos database, open squares indicate the subset used in Christensen & Aubert (2006).

The statistical balance between both terms of the right-hand side of the dimensional form of the induction equation (2) yields to  $uB/\ell \sim \eta B/\ell_B^2$ , where we introduced a typical velocity field strength  $u$ , and  $\ell$  has the dimension of a length scale which depends on correlations between the norm and direction of  $\mathbf{u}$  and  $\mathbf{B}$ . The length scales  $\ell_B$  and  $\ell$  are thus related by

$$\ell_B \sim \eta^{1/2} u^{-1/2} \ell^{1/2}, \quad (15)$$

which can be normalised as

$$\ell_B^* \sim \text{Rm}^{-1/2} \ell^{*1/2}, \quad \text{or} \quad \ell_B^* \sim E_\eta^{1/2} \text{Ro}^{-1/2} \ell^{*1/2}, \quad (16)$$

where  $\text{Rm}$  is the magnetic Reynolds number, and  $\text{Ro}$  is the Rossby number, defined as  $\text{Ro} \equiv (2 E_{\text{kin}}^*/V^*)^{1/2} \equiv u^*$ ,

$$\text{with} \quad E_{\text{kin}} \equiv \int_V \frac{\rho \mathbf{u}^2}{2} dV \quad \text{i.e.} \quad E_{\text{kin}}^* \equiv \int_V \frac{\mathbf{u}^{*2}}{2} dV^*. \quad (17)$$

The magnetic dissipation length scale  $\ell_B$  is thus an output parameter, in so far as it is related to both the characteristic velocity  $u$  of the flow (measured by  $\text{Ro}$  or  $\text{Rm}$ ) and the length scale  $\ell$  (see appendix C.1).

### 3.4 Existing scaling laws for the magnetic field strength and their physical interpretation

Christensen & Aubert (2006) introduced two seminal scaling laws

$$\text{Lo} \sim f_{\text{ohm}}^{1/2} \text{Ra}_Q^{*0.34}, \quad (18)$$

and its optimised form

$$\text{Lo} \sim f_{\text{ohm}}^{1/2} \text{Ra}_Q^{*0.32} \text{Pm}^{0.11}. \quad (19)$$

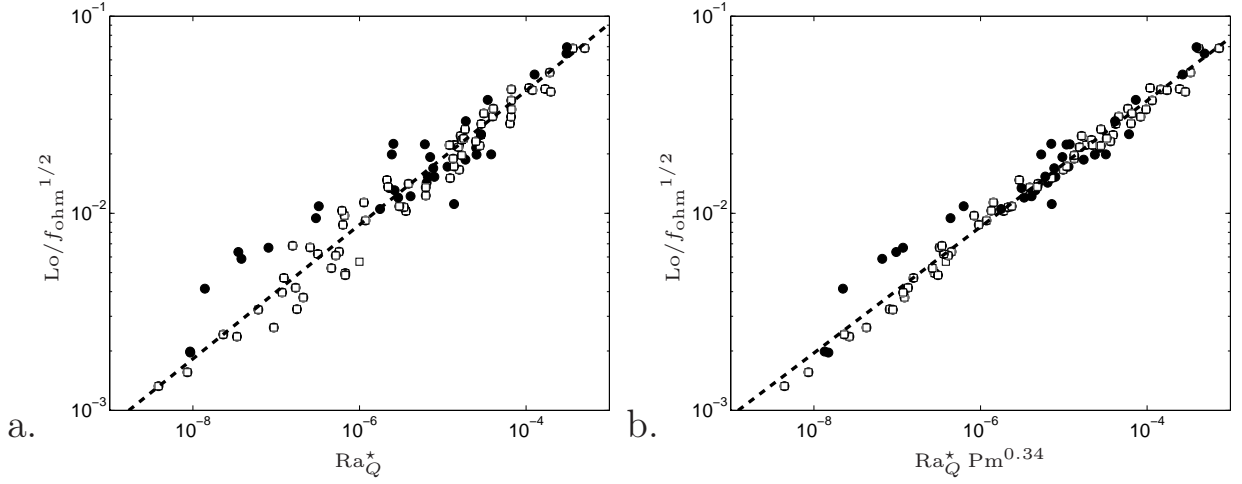


Figure 2: The Lorentz number corrected for the relative fraction of Ohmic dissipation versus a combination of the flux-based Rayleigh number and the magnetic Prandtl number, as proposed by Christensen & Aubert (2006): (a) relation (18), (b) relation (19). Black points correspond to the 102 dynamos database, open squares indicate the subset of data used in Christensen & Aubert (2006).

Their application to the 102 dynamos database is represented in figure 2, and yields the relative misfits  $\chi_{\text{rel}} = 0.256$ , and  $\chi_{\text{rel}} = 0.152$  respectively. The corresponding assumption on the magnetic dissipation length scale  $\ell_B^*$  is detailed in appendix C.2. It respectively yields

$$\ell_B^* \sim \text{Ra}_Q^{*-0.16} E_\eta^{1/2}, \quad \text{and} \quad \ell_B^* \sim \text{Ra}_Q^{*-0.18} E_\eta^{1/2} \text{Pm}^{-0.39}, \quad (20)$$

which are represented in figure 3 (see appendix C.2 for discussion).

Relation (18) and its optimised form (19) are empirical laws obtained using numerical experiments. The physical interpretation of relation (18), as provided by Christensen & Aubert (2006), is based on two assumptions: the empirical scaling law for the magnetic dissipation time  $\tau_\eta^* \sim \text{Rm}^{-1}$  (Christensen & Tilgner, 2004), which is equivalent to assuming  $\ell^* \sim 1$  (see appendix C.1), and their empirical fit  $\text{Ro} \sim \text{Ra}_Q^{*0.41}$  (equation (30) in Christensen & Aubert, 2006). Using equation (16), these two assumptions provide  $\ell_B^* \sim \text{Ra}_Q^{*-0.21} E_\eta^{1/2}$ . This last expression can then be injected in equation (10), to yield  $\text{Lo} \sim f_{\text{ohm}}^{1/2} \text{Ra}_Q^{*0.29}$ . Thus, their demonstration leads to an exponent of  $\text{Ra}_Q^*$  equal to 0.29, which is only slightly lower than their optimal exponent 0.34 in (18).

Christensen (2010) proposed a modified interpretation: while retaining the assumption  $\ell^* \sim 1$ , he replaced the scaling law for  $\text{Ro}$  by the one resulting from mixing length theory (balance between inertia and buoyancy). This theory, usually applied for turbulent convection in stars (Stevenson, 1979; Kippenham & Weigert, 1990), provides  $\text{Ro} \sim \text{Ra}_Q^{*1/3}$ . It leads to  $\text{Lo} \sim f_{\text{ohm}}^{1/2} \text{Ra}_Q^{*1/3}$ , which is closer to the original fit (18) obtained by Christensen & Aubert (2006). Instead, Jones (2011) based his physical reasoning on the inertial scaling law  $\text{Ro} \sim \text{Ra}_Q^{*2/5}$  (derived from the so-called IAC balance, see Aubert et al., 2001), and obtained  $\text{Lo} \sim f_{\text{ohm}}^{1/2} \text{Ra}_Q^{*0.30}$ . The assumptions of inertial scaling laws for  $\text{Ro}$  made by both Christensen (2010) and Jones (2011) however do not seem relevant to dipolar numerical dynamos (see section 4.5 of this paper; and Christensen & Aubert, 2006; Soderlund et al., 2012).

More recently, Davidson (2013) studied analytically the asymptotic limit expected to be relevant to planetary dynamos. In this limit, viscosity is negligible, which implies a vanishing viscous dissipation ( $f_{\text{ohm}} \sim 1$ ), and inertial forces do not enter the dominant forces balance (small Rossby number limit). Davidson's argument relies on a dimensional analysis. On the right-hand side of equation (9), with  $f_{\text{ohm}} = 1$ , both  $\text{P}_M$  and  $\ell_B^2/\eta$  are assumed to be independent on  $\Omega$ . This implies that  $B^2/(\rho\mu)$

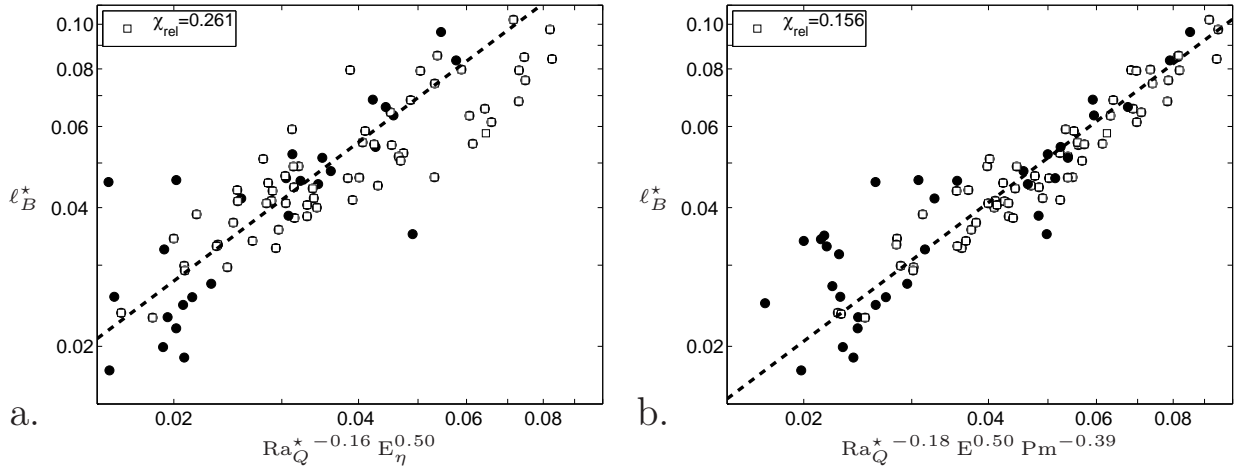


Figure 3: The magnetic dissipation length scale versus a combination of the flux-based Rayleigh number, the Ekman number and the magnetic Prandtl number, as implied by Christensen & Aubert (2006) results (relations (20)). Black points correspond to the full 102 dynamos database, open squares indicate the subset used in Christensen & Aubert (2006).

only depends on  $L$  and  $P_M$ , and thus

$$\frac{B^2}{\rho \mu} \sim L^{2/3} P_M^{2/3}, \quad (21)$$

(see equation (6) in Davidson, 2013). In order to account for viscous effects in numerical simulations, Davidson (2013) then replaces  $P_M$  with  $f_{\text{ohm}} P_M$  in (21), which leads to

$$\frac{B^2}{\rho \mu} \sim L^{2/3} (f_{\text{ohm}} P_M)^{2/3}, \quad (22)$$

(equation (9) in Davidson, 2013). It can be rewritten in its non-dimensional form as

$$\text{Lo} \sim f_{\text{ohm}}^{1/3} \text{Ra}_Q^*{}^{1/3}. \quad (23)$$

Note that relation (23) is based on physical considerations valid for the Earth's core but not necessarily realised in direct numerical simulations (see appendix D). It is similar to (18) except for the exponent of  $f_{\text{ohm}}$ . The importance of this measured quantity in the efficiency of the power based scaling laws is investigated in appendix B. Its application to the 102 dynamos database is represented in figure 4, and yields a relative misfit  $\chi_{\text{rel}} = 0.286$ .

We discussed above three scaling laws proposed for the magnetic field strength primarily as a function of the available power generated by buoyancy forces and corresponding to equations (18), (19) and (23). Their application to our dynamos database is represented in figures 2 and 4. Note that extending the 65 dynamos database of Christensen & Aubert (2006) to the 102 dynamos database provided by U. Christensen and used in the present paper, leads to a lower quality fit for the magnetic field amplitude (compare figures 8-9 in Christensen & Aubert, 2006, with figures 2.a,b in the present paper). The three relations offer a good description of the available numerical data, with relative misfits between 0.15 and 0.30. The best one is naturally relation (19), since it involves a supplementary parameter  $P_m$  compared to scaling laws (18) and (23).

It is interesting to compare these three relations with the most simple form which stems from the energy balance between production and dissipation and the assumption that  $\ell_B$  is constant (dominant dipole field). This expression is represented in figure 1 (see also equation (14)). The relative misfit is

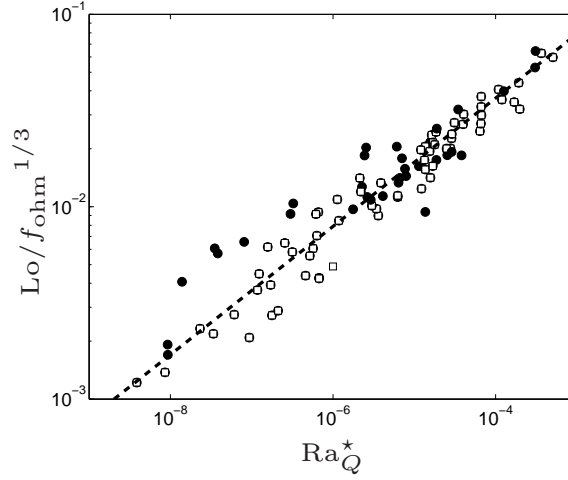


Figure 4: The Lorentz number corrected for the relative fraction of Ohmic dissipation versus a combination of the flux-based Rayleigh number and the magnetic Prandtl number, as proposed by Davidson (2013), relation (23). Black points correspond to the 102 dynamos database, open squares indicate the subset of data used in Christensen & Aubert (2006).

only improved by some 50% from this last relation to relations (18), (19) and (23) which all attempt to a finer description of the magnetic dissipation length scale. The range of variation of  $\ell_B$  in numerical models is necessarily restricted between the discretisation size and the size  $L$  of the model. The key assumption is thus the statistical balance between energy production and dissipation, which is bound to work for any statistically steady dynamo (as illustrated in figure 1). This explains why the power based scaling law (18) was found to work with different prefactors for dipolar and multipolar dynamos, despite of their different induction mechanisms (Christensen, 2010; Schinnerer et al., 2012).

## 4 Predictive scaling laws for the magnetic field strength

Power based scaling laws, discussed in the previous section, properly describe the numerical database. However they only relate together measured quantities. We now want to express scaling laws which only involve input parameters on the right-hand side. Such scaling laws will be referred to as “predictive” in the sense that they estimate the strength of a measured quantity, say the magnetic field strength, as a function of input parameters only (i.e. parameters that explicitly enter the governing equations), and can therefore be used before any simulation is performed (as opposed to scaling laws involving measured quantities such as  $Ra_Q^*$  and  $f_{ohm}$ ).

### 4.1 Control parameters

Only four non-dimensional parameters can be introduced in the governing equations (1-3). In our formulation, these are the Ekman number  $E$ , the Prandtl number  $Pr$ , the magnetic Prandtl number  $Pm$  and the Rayleigh number  $Ra$  (see section 2). According to the Buckingham  $\pi$  theorem, any additional non-dimensional quantity, e.g. the Elsasser number  $\Lambda \equiv Lo^2 Pm/E$ , can therefore be expressed as a function of the above four non-dimensional control parameters. The choice of non-dimensional parameters is however non-unique (for example, the Roberts number  $q = \kappa/\eta$  could be used instead of the magnetic Prandtl number  $Pm = \nu/\eta$ ).

Stelzer & Jackson (2013) opened the way to a predictive scaling by expressing  $Nu - 1$ ,  $Ro$  and  $Lo/f_{ohm}^{1/2}$  as a function of  $Ra$  instead of  $Ra_Q^*$  (see their section 5). Their approach however is bound



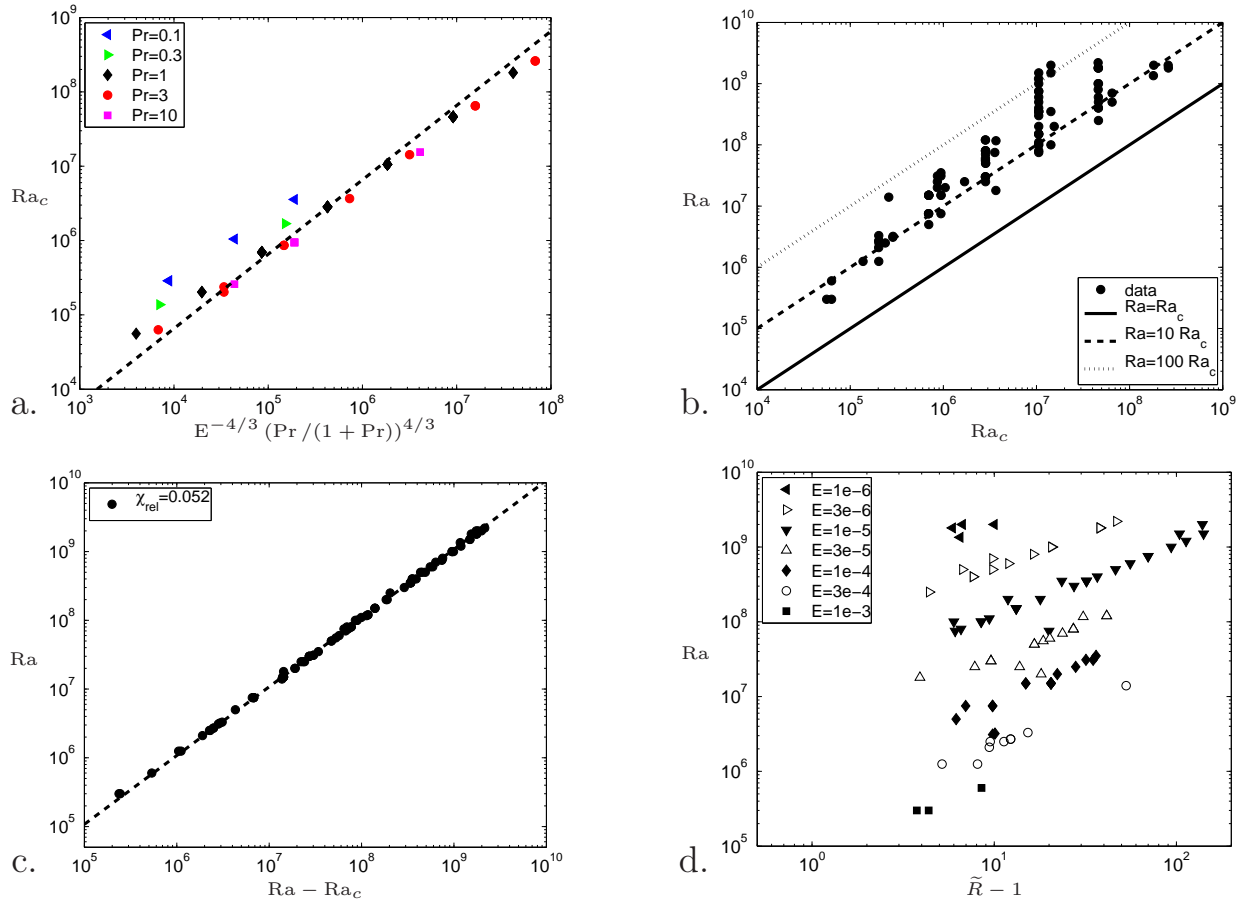


Figure 5: (a) The critical Rayleigh number for the onset of convection versus the predicted combination of the Ekman number and the Prandtl number (Busse, 1970). (b) Parameter range: Rayleigh number in ordinate, critical Rayleigh number for convection in abscissa. (c) The strong correlation in the database between the Rayleigh number and its distance to the onset of convection. (d) The Rayleigh number versus its normalised distance to the onset of convection. The four graphs rely on the 102 dynamos database.

to fail for small values of  $Ra$  as all these measured quantities obviously vanish below the onset of convection or dynamo action.

Instead of using the Rayleigh number as control parameter, it is thus natural to introduce the distance to an instability threshold. We thus introduce  $Ra_c$  and  $Ra_d$ , which respectively correspond to the onset of convection and dynamo action (see appendix E for  $Ra_d$ ). The measured quantities  $Nu - 1$  and  $Ro$  are expected to vanish at the onset of convection  $Ra = Ra_c$  and  $Lo$  at the onset of dynamo action  $Ra = Ra_d$ .

The quantity  $Ra - Ra_c$  therefore provides a natural control parameter for hydrodynamic quantities such as  $Nu - 1$  and  $Ro$ . This control parameter, even though natural, is however biased because of the strong dependence of the critical Rayleigh number  $Ra_c$  on  $E$  and  $Pr$ . This dependence, first formulated and investigated by Chandrasekhar (1961) in the cartesian geometry, has been extensively studied. Especially, Roberts (1968) then Busse (1970) studied the limit  $E \ll 1$  in a spherical geometry. In a perturbative cylindric model for a uniformly heated fluid, Busse (1970) proposed

$$Ra_c \sim E^{-4/3} \left( \frac{Pr}{1 + Pr} \right)^{4/3}. \quad (24)$$

This solution, valid in the limit of asymptotic Ekman numbers, is consistent with several other studies:

e.g. Carrigan & Busse (1983) (experimental convection study in a differentially heated spherical shell), Jones et al. (2000) (uniformly heated fluid in a sphere), Takehiro et al. (2002) (fixed heat flux boundary conditions), Dormy et al. (2004) and Zhang & Liao (2004). It is validated to a certain extent against the finite Ekman number numerical database used in this paper. The corresponding misfit is  $\chi_{\text{rel}} = 0.319$  and it is represented in figure 5.a. Note that a dependence on  $\text{Pr}/(1 + \text{Pr})$  remains. The optimised scaling law obtained with our database is  $\text{Ra}_c \simeq 17.78 \text{E}^{-1.19} (\text{Pr}/(1 + \text{Pr}))^{0.58}$ , with  $\chi_{\text{rel}} = 0.061$  (95% confidence intervals in table 2): optimised exponents are slightly weaker (in absolute value) than those predicted by the asymptotic calculus of Busse (1970), which indicates that these models are still not in an asymptotic limit.

In practice, the numerical experiments used in this study are performed for values of  $\text{Ra}$  of the order of 10 times the critical value (see figure 5.b). Indeed, only dynamos with  $\text{Nu} > 2$  are considered in the database (see Christensen & Aubert, 2006), on the other hand, for obvious computational reasons associated with small scale motions,  $\text{Ra}$  is never very far from the onset in numerical models. As a result, the values of  $\text{Ra}$  are strongly correlated with the values of  $\text{Ra}_c$ . It follows that  $\text{Ra}$  is in fact close to  $\text{Ra} - \text{Ra}_c$ : in the numerical database,  $\text{Ra} \approx 1.11(\text{Ra} - \text{Ra}_c)$  with a relative misfit  $\chi_{\text{rel}} = 0.052$  (see figure 5.c). This last relation, which traduces a bias in the database, explains why Stelzer & Jackson (2013) obtained satisfying fits of  $\text{Ro}$  and  $\text{Nu} - 1$  as a function of  $\text{Ra}$  (without introducing the distance to the onset of convection).

The strong dependence of  $\text{Ra}_c$  on the Ekman number introduces a very large variation of the control parameter  $\text{Ra} - \text{Ra}_c$ , spanning over five orders of magnitude in the numerical database. This is somewhat fictitious as the parameter  $\text{Ra}/\text{Ra}_c$  would only vary over one order of magnitude. We thus introduce  $\tilde{R} \equiv \text{Ra}/\text{Ra}_c$  and our new control parameter will thus be  $\tilde{R} - 1$  (as  $\tilde{R}_c = 1$ ). This new control parameter filters out the Ekman and Prandtl number dependences (the Ekman dependence is highlighted in figure 5.d).

To measure the distance to the onset of dynamo action, we also introduce the control parameter  $\tilde{R} - \tilde{R}_d$ , where  $\tilde{R}_d \equiv \text{Ra}_d/\text{Ra}_c$  is a function of  $\text{E}$ ,  $\text{Pr}$  and  $\text{Pm}$  only. Nevertheless, whereas  $\text{Ra}_c$  is known for all numerical experiments in the database provided by U. Christensen, this is not the case for the critical value at the onset of dynamo action  $\text{Ra}_d$ . It can be estimated through a linear interpolation of  $\text{Lo}^2$  as a function of  $\text{Ra}$  near the onset of dynamo action (see appendix E). Such an estimate could only be performed for seven sets of  $\text{E}$ ,  $\text{Pr}$  and  $\text{Pm}$  in the database (see table 1), which corresponds to 33 numerical simulations. It is extended to 42 simulations thanks to 9 additional direct numerical simulations extracted from Morin & Dormy (2009) and corresponding to the set  $\text{E} = 3 \times 10^{-4}$ ,  $\text{Pr} = 1$ ,  $\text{Pm} = 3$ .

Our four control parameters therefore are: the Ekman number  $\text{E}$ , the Prandtl number  $\text{Pr}$ , the magnetic Prandtl number  $\text{Pm}$  and the relative distance to either the onset of convection or of dynamo action,  $\tilde{R} - 1$  and  $\tilde{R} - \tilde{R}_d$  respectively.

## 4.2 Direct numerical fit versus forces balances

Empirical scaling laws deduced from the multiple linear regression method applied to numerical data have to be considered carefully for two main reasons. First, the ranges of some input parameters are highly correlated, which introduces bias in scaling laws. It is the case for the Ekman number and the magnetic Prandtl number. The minimal value of  $\text{Pm}$  required for dynamo is indeed dependent on  $\text{E}$  (see Christensen & Aubert, 2006). Figure 6 represents the range of  $\text{Pm}$  as a function of the range of  $\text{E}$  in the 102 dynamos database used in the present study: the minimal value of  $\text{Pm}$  varies roughly as  $\text{E}^{3/4}$  (Christensen et al., 1999; Christensen & Aubert, 2006), although this cannot be distinguished from  $\text{E}^{2/3}$  (as proposed by Dormy & Le Mouél, 2008). As a consequence, the scaling laws obtained via a direct numerical fit have to be considered carefully. In particular, biases can occur relating

E	Pr	Pm	Ra <sub>d</sub>	Rm <sub>d</sub>
$3 \times 10^{-4}$	1	3	$6.125 \times 10^5$	62.5
$1 \times 10^{-4}$	1	0.5	$3.6 \times 10^6$	26
$1 \times 10^{-4}$	1	1	$2.4 \times 10^6$	34
$1 \times 10^{-4}$	10	10	$5 \times 10^5$	25
$3 \times 10^{-5}$	1	0.25	$2.6 \times 10^7$	29
$3 \times 10^{-5}$	1	1	$1.5 \times 10^7$	70
$3 \times 10^{-5}$	1	2.5	$1.04 \times 10^7$	103
$1 \times 10^{-5}$	1	0.5	$8.0 \times 10^7$	70
$1 \times 10^{-5}$	1	1	$4.7 \times 10^7$	68
$1 \times 10^{-5}$	1	2	$4.9 \times 10^7$	150
$3 \times 10^{-6}$	1	0.1	$6.4 \times 10^8$	40
$3 \times 10^{-6}$	1	0.5	$2.4 \times 10^8$	60

Table 1: Estimated values of the Rayleigh number and of the magnetic Reynolds number, corresponding to the onset of dynamo action (see appendix E).

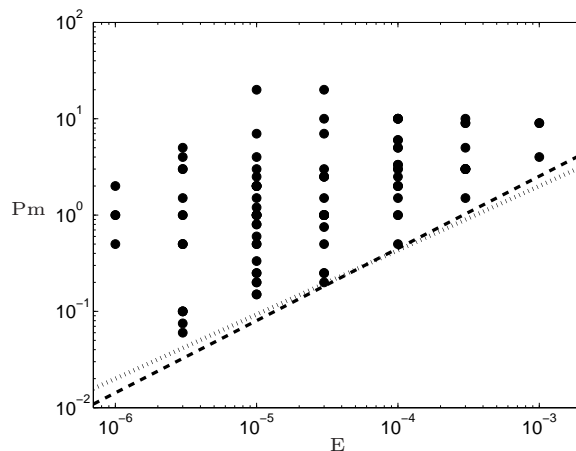


Figure 6: Correlation in control parameters used in numerical models; the magnetic Prandtl number is represented as a function of the Ekman number. The dashed line corresponds to  $Pm_{\min} = 450 E^{0.75}$  (Christensen & Aubert, 2006) and the dotted line to  $Pm_{\min} \sim E^{2/3}$  (Dormy & Le Mouél, 2008). This figure relies on the full 102 dynamos database.

dependences on  $E$  and  $Pm$ .

The second important limit of the approach based on empirical scaling laws deals with the restriction of our scaling analysis to power laws. In particular, the dependence on the Prandtl coefficient seems more complex than a simple power law. For instance, the dependence of the critical Rayleigh number  $Ra_c$  on  $Pr$  takes the form  $Pr/(1+Pr)$  (see (24) above). Indeed, a power law expression would diverge in the limit  $Pr$  tends to infinity.

Because of the above limitations, we prefer to guide our derivation of scaling laws with physical arguments such as forces balances. Our motivation is to take some distance with empirical fits, and to rely on the numerical database to validate the proposed scaling laws, guided by physical arguments.

### 4.3 Magnetic field strength as a function of the flow amplitude

A first step in our reasoning consists in expressing the magnetic field strength as a function of the flow amplitude. In experimental physics, one usually controls the peak velocity of a flow driven

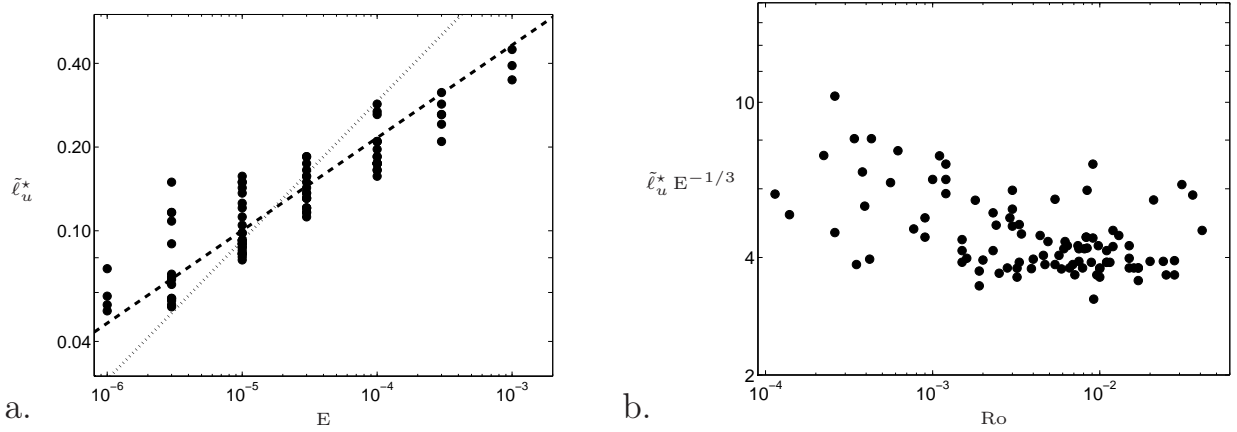


Figure 7: (a) The non-dimensional characteristic length scale  $\tilde{\ell}_u^*$  as a function of the Ekman number. The dashed line corresponds to  $\tilde{\ell}_u^* \sim E^{1/3}$  (equation (27)) and the dotted line to  $\tilde{\ell}_u^* \sim E^{1/2}$ . (b) The corrected length scale  $\tilde{\ell}_u^* E^{-1/3}$  as a function of the Rossby number. Similar graphs can be produced using  $\ell_u^*$  instead of  $\tilde{\ell}_u^*$ . This figure relies on the full 102 dynamos database.

say by propellers. For this reason, earlier theoretical work often focused on the relation between the produced magnetic field and the velocity field. A first approach is to consider dynamos which bifurcate from a laminar flow. One assumes that in such cases, a dominant balance exists between the Lorentz force and the viscous force associated to the flow modification (Petrelis & Fauve, 2001).

It yields the equilibrium

$$\text{Lo}^2 \sim E \frac{\text{Ro} - \text{Ro}_d}{\tilde{\ell}_u^{*2}}, \quad (25)$$

where  $\text{Ro}_d$  corresponds to the Rossby number at the onset of dynamo action, and the length scale  $\tilde{\ell}_u$  corresponds to the characteristic length scale of the flow calculated as the mean scale of the kinetic energy spectrum (see Christensen & Aubert, 2006). This length scale is very similar to our  $\ell_u$  introduced in appendix B.1.

Supposing, as do Petrelis & Fauve (2001), that  $\tilde{\ell}_u^* \sim 1$ , this leads in non-dimensional form to

$$\Lambda \sim (\text{Rm} - \text{Rm}_d) E, \quad (26)$$

where  $\text{Rm}_d$  corresponds to the critical value of  $\text{Rm}$  at the onset of dynamo action.

While the length scale  $\tilde{\ell}_u^*$  necessarily varies over a limited range in the numerical database (see figure 7.a and the discussion at the end of section 3.4), a finer description can be achieved by retaining viscous effects and neglecting inertial forces. The equilibrium between the curl of the Coriolis force and the viscous force indeed yields

$$\tilde{\ell}_u^* \sim E^{1/3}. \quad (27)$$

This last relation properly describes the database used in the present paper, as shown in figure 7.a and in King & Buffett (2013) (see also Roberts & King, 2013). The lengthscale  $\tilde{\ell}_u^*$  clearly depends on  $E^{1/3}$  and not on  $E^{1/2}$ , the latter being the typical scale of boundary layers. Thus, viscous effects play a non-negligible role in the bulk of the flow. This indicates that present numerical simulations are not in a dynamical regime relevant to the Earth's core (see also Soderlund et al., 2012). The  $E^{1/3}$  scale would represent less than 100m for geophysical values. Besides, the mild dependence of  $\tilde{\ell}_u^* E^{-1/3}$  on the Rossby number (see figure 7.b) shows that the assumption that inertia is small compared to viscous effects is verified by numerical models.

If one uses (27) for the length scale  $\tilde{\ell}_u^*$  in relation (25) (see Fauve & Petrelis, 2007), this yields

$$\Lambda \sim (\text{Rm} - \text{Rm}_d) E^{1/3}. \quad (28)$$

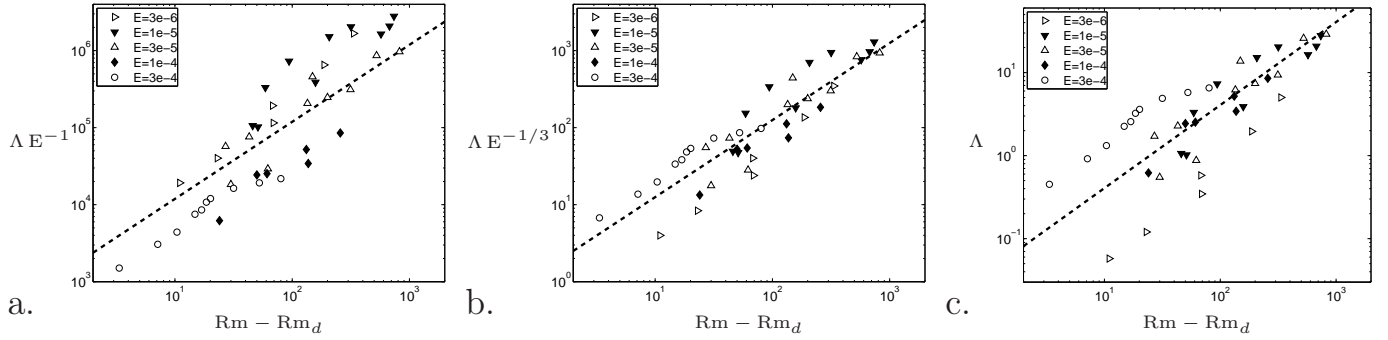


Figure 8: Scaling laws for the magnetic field strength as a function of the flow amplitude as measured by  $Rm - Rm_d$ : (a) relation (26), (b) relation (28) and (c) relation (29). This figure relies on the 42 dynamos database.

An alternative forces balance, known as the strong field balance, and assumed to be valid for the Earth's core, consists in assuming a balance between the Lorentz force and the modification of the Coriolis force. It provides (see Petrelis & Fauve, 2001) in non-dimensional form

$$\Lambda \sim (Rm - Rm_d). \quad (29)$$

Each of the relations (26), (28) and (29) can be tested against the 42 dynamos database (see figure 8), and yields the relative misfits  $\chi_{\text{rel}} = 1.438$ ,  $\chi_{\text{rel}} = 0.891$ , and  $\chi_{\text{rel}} = 2.081$  respectively. The best scaling law fitting the numerical data is therefore (28). It is consistent with the fact that viscous effects have been shown to play a non-negligible role in the bulk of the flow in numerical models.

This result can be compared to the output of a direct numerical fit. The values of the magnetic Reynolds number at the onset of dynamo action corresponding to seven sets of  $E$ ,  $Pr$  and  $Pm$  in the database have been estimated by a linear interpolation of  $Lo^2$  as a function of  $Rm$  (see table 1 and appendix E). The multiple linear regression approach applied to the 42 dynamos database provides the following scaling law for the Elsasser number  $\Lambda$  as a function of  $(Rm - Rm_d)$  and  $E$  (95% confidence intervals given in table 3):<sup>1</sup>

$$\Lambda \simeq 10.24 (Rm - Rm_d)^{1.09} E^{0.52}, \quad \text{with } \chi_{\text{rel}} = 0.698. \quad (30)$$

The physically derived scaling law (28) is consistent with the empirical scaling law (30) for the dependence on  $(Rm - Rm_d)$ . The optimal exponent of  $E$  is larger than the  $1/3$  value predicted by (28), and remains to be investigated.

Figure 10.a represents relation (28) applied to the 42 dynamos database in red diamonds, and the same relation, but setting  $Rm_d$  to zero in blue squares. The blue points gradually move away from a linear fit when  $Rm$  decreases, as expected (because the approximation  $Rm - Rm_d \simeq Rm$  worsens). Relation (28) can however then be applied to the 102 dynamos database, provided that the parameter  $Rm_d$  is dropped (since it is only known for the 42 simulations of the reduced database). It is represented in figure 10.b. As in figure 10.a, the full numerical database appears to follow the proposed scaling law, except for low values of  $Rm$  for which  $Rm_d$  cannot be neglected.

<sup>1</sup> A direct numerical fit of  $\Lambda$  as a function of  $(Rm - Rm_d)$ ,  $E$ ,  $Pm$  and  $Pr$  yields  $\Lambda \simeq 0.30 (Rm - Rm_d)^{0.88} E^{0.12} Pm^{0.79} Pr^{-0.82}$ , with  $\chi_{\text{rel}} = 0.301$  (see table 3 and figure 9.a). The proposed dependence on  $Pr$  is not strongly constrained, since the estimation of the optimal exponent of  $Pr$  is only based on 3 simulations corresponding to  $Pr \neq 1$  (and for all three,  $E = 1 \times 10^{-4}$ ,  $Pr = 10$ ,  $Pm = 10$ , see table 1). The proposed dependence is therefore clearly not robust. The bias between  $E$  and  $Pm$  in the database probably accounts for the smaller exponent of  $E$  and the extra dependence on  $Pm$  in the above relation compared to (30).

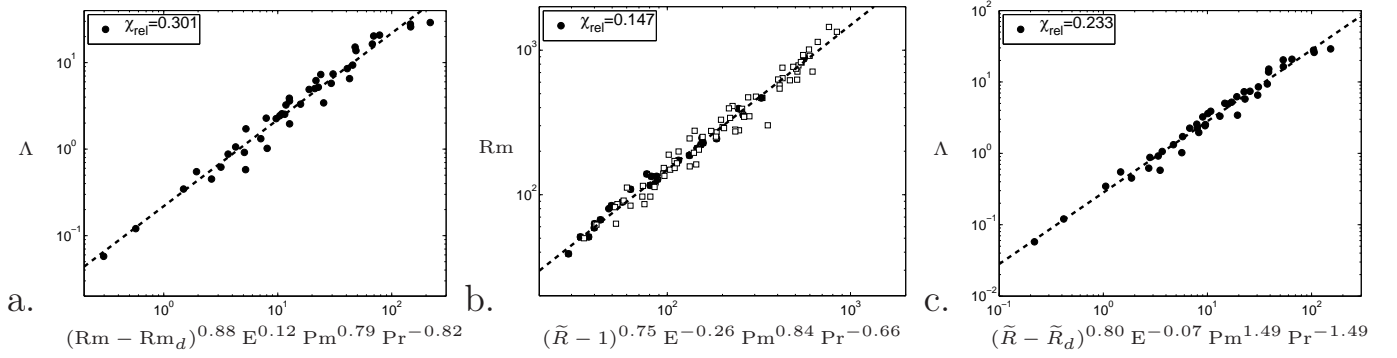


Figure 9: Scaling laws provided by direct numerical fits. (a) The Elsasser number versus the flow amplitude (see footnote 1). (b) The magnetic Reynolds number versus the normalised distance to the onset of convection (see footnote 4). (c) Predictive scaling law for the Elsasser number versus the normalised distance to the onset of dynamo action (relation (40)). Squares correspond to the 102 dynamos database, black points to the 42 runs of the reduced database.

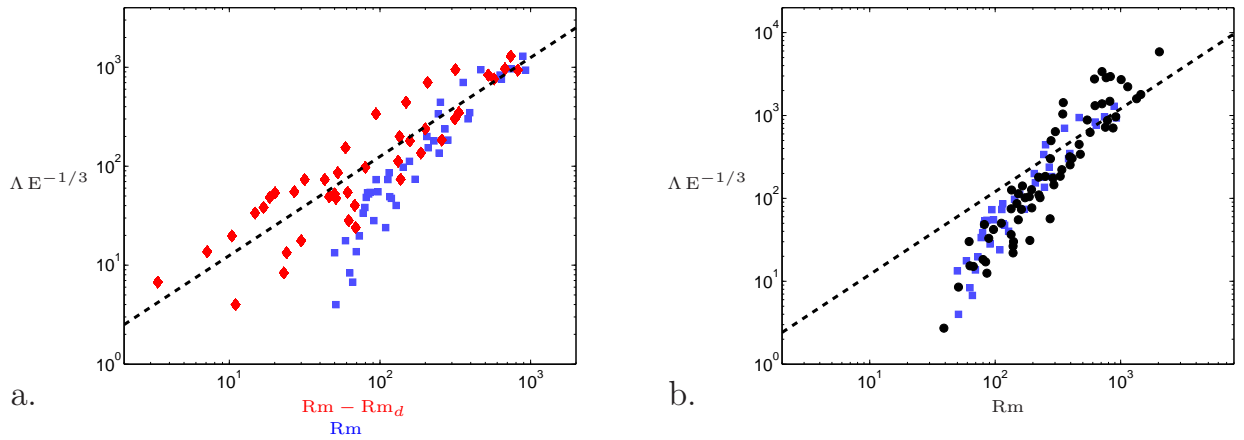


Figure 10: Physically derived relation for the magnetic field strength as a function of  $Rm - Rm_d$ . (a) Relation (28) (red diamonds), and the same relation but setting  $Rm_d$  to zero (blue squares), both applied to the 42 dynamos database. (b) Relation (28) dropping the unknown  $Rm_d$  contribution, applied to the full (black points) and reduced (blue squares) database. The dashed line corresponds to relation (28).

It is worth noting that relation (28) reveals a dependence of the magnetic field strength on viscosity, which is geophysically not realistic. To illustrate this, let us now try to apply this relation to the Earth's core. We choose the common estimate value  $Rm = 10^3$ . The distance to the onset of dynamo action  $Rm - Rm_d$  can be estimated by  $Rm$ , which leads to an over-estimated value of  $\Lambda$ . We find  $\Lambda \sim 10^{-2}$ , which is an upper bound because  $Rm_d$  was not taken into account. It is yet much smaller than its estimated value for the Earth's core, expected to be close to unity (Roberts, 1988). This indicates very clearly that available numerical models are not in the dynamical regime relevant to geodynamo. In other words, the Earth's core would simply be out of the range of figure 10.a (with  $Rm \simeq 10^3$ , and  $\Lambda E^{1/3} \simeq 10^5$ ).

The magnetic Reynolds number is however a measured quantity in the numerical database. In order to establish a predictive scaling for the magnetic field strength, it is thus necessary to express the flow amplitude as a function of control parameters. This is the purpose of the two next sections.

## 4.4 Predictive scaling law for the injected power

The definition of the output parameter  $\text{Ra}_Q^*$  involves the efficiency with which heat is transferred by convection, measured by the Nusselt number  $\text{Nu}$  (see equation (13)). This is a subject of study in itself, many studies of heat transfer have been performed for rotating convection. Figure 11 shows that the numerical data globally correspond to an intermediate regime between the rapidly rotating regime ( $\text{Nu} = \tilde{R}^{6/5}$ , Aurnou, 2007; King et al., 2009, 2010) and the weakly rotating regime ( $\text{Nu} \sim \text{Ra}^{2/7}$ , see King et al., 2009). The simple relation  $\text{Nu} \sim \tilde{R}$  provides a good description of the database. Note that in figure 11, a dependence on  $\text{Pr}$  remains. This could be further investigated by seeking for a dependence on  $\text{Pr}/(1 + \text{Pr})$  (instead of a power law dependence which would lack regularity in the limit  $\text{Pr} \rightarrow 0$  or  $\text{Pr} \rightarrow +\infty$ ). As we will however discuss later (see section 4.6), the  $\text{Pr}/(1 + \text{Pr})$  term can be omitted without significant loss of quality in describing the present database.

In the available database, the bias  $\text{Ra} \sim \text{Ra} - \text{Ra}_c$  (see section 4.1) allows us to approximate  $\text{Ra}$  by  $(\tilde{R} - 1) \text{Ra}_c$  in the definition (13) of  $\text{Ra}_Q^*$ . Injecting (24) and the above simple expression for  $\text{Nu}$  (which is admittedly not based on solid physical considerations) yields

$$\text{Ra}_Q^* \sim (\tilde{R} - 1)^2 \text{E}^{5/3} \text{Pr}^{-2} \left( \frac{\text{Pr}}{1 + \text{Pr}} \right)^{4/3}. \quad (31)$$

The corresponding relative misfit when applied to the 102 dynamos database is  $\chi_{\text{rel}} = 0.311$  and it is represented in figure 12.a. Note that the dependence on  $\text{Pr}^{-2}$  in (31) comes from the definition (13) of  $\text{Ra}_Q^*$ , whereas that on  $(\text{Pr}/(1 + \text{Pr}))^{4/3}$  results from the expression of  $\text{Ra}_c$  (relation (24)).

Relation (31) can be compared to an optimised empirical fit, which provides

$$\text{Ra}_Q^* \simeq 5.10 (\tilde{R} - 1)^{1.78} \text{E}^{1.70} \text{Pr}^{-2.12} \left( \frac{\text{Pr}}{1 + \text{Pr}} \right)^{1.26}, \quad \text{with } \chi_{\text{rel}} = 0.173, \quad (32)$$

(95% confidence intervals are given in table 2). Relation (31) is therefore close to providing the best fit through the numerical database.<sup>2</sup>

The parameter  $\text{Ra}_Q^*$  varies over six orders of magnitude, while none of the control parameters varies over such a wide range (see appendix C.2). Figure 12.b highlights the strong dependence of  $\text{Ra}_Q^*$  on the Ekman number explicited in (31). This explains the above range of variation. The control parameter  $\tilde{R} - 1$  covers a much more physically realistic range.

## 4.5 Predictive scaling laws for the flow amplitude

Several scaling laws based on different forces balances have been proposed in the literature concerning the flow amplitude (detailed in King & Buffett, 2013). For simulations near the onset of dynamo action, the Lorentz force can be expected to be small. Then, balancing the curl of the buoyancy term with that of the Coriolis force yields

$$u^* \sim \tilde{\ell}_u^{*-1} \frac{\text{P}^*}{u^*}, \quad (33)$$

which can be rewritten, using relation (12), as

$$\text{Ro} \sim \tilde{\ell}_u^{*-1/2} \text{Ra}_Q^{*1/2}. \quad (34)$$

---

<sup>2</sup> If the dependence on  $\text{Pr}/(1 + \text{Pr})$  is omitted, it yields a larger misfit ( $\chi_{\text{rel}} = 0.326$ ), and  $\text{Ra}_Q^* \simeq 1.47 (\tilde{R} - 1)^{1.77} \text{E}^{1.68} \text{Pr}^{-1.56}$ . Both relations would not be modified if a dependence on  $\text{Pm}$  was sought (see table 2).

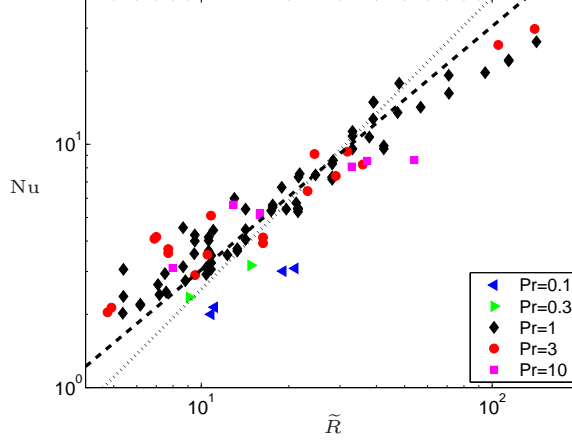


Figure 11: The Nusselt number versus the Rayleigh number normalised by its critical value. The dotted line corresponds to  $Nu \sim \tilde{R}^{6/5}$  and the dashed line to  $Nu \sim \tilde{R}$ . The Prandtl number is indicated by the color (as in figure 5.a). This figure is based on the 102 dynamos database.

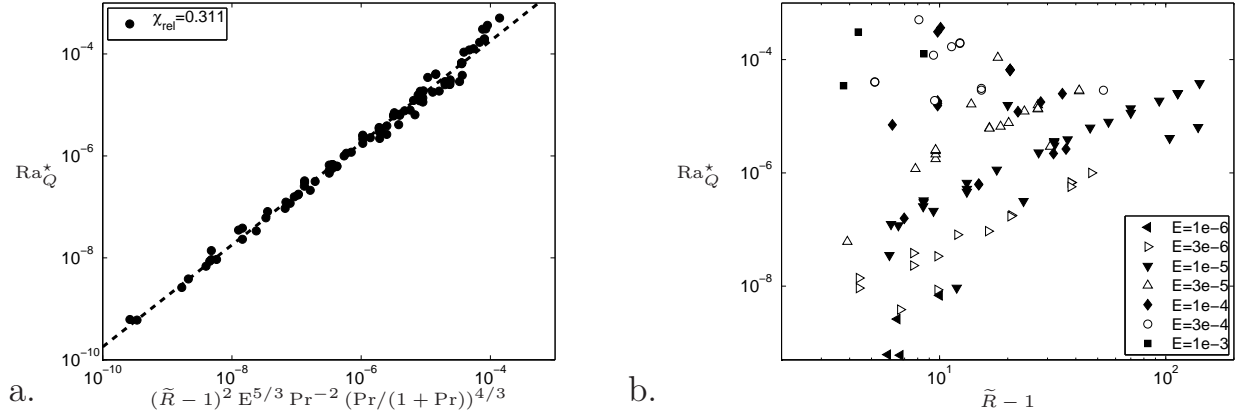


Figure 12: (a) Validation of relation (31) expressing the flux-based Rayleigh number as a function of the normalised distance to the onset of dynamo. (b) The flux-based Rayleigh number versus the normalised distance to the onset of convection. The Ekman number is indicated by using different symbols (as in figure 5.d). This figure is based on the full 102 dynamos database.



	Pre-factor	$\text{Ra}_Q^*$	$\tilde{R} - 1$	E	Pm	Pr	$\text{Pr}/(1 + \text{Pr})$	$\chi_{\text{rel}}$
$\text{Ra}_c$	$17.779 \pm 1.468$	×	×	$-1.193 \pm 0.008$	×	×	$0.579 \pm 0.030$	0.061
$\text{Ra}_Q^*$	$1.470 \pm 0.517$	×	$1.774 \pm 0.064$	$1.675 \pm 0.032$	-	$-1.557 \pm 0.061$	×	0.326
$\text{Ra}_Q^*$	$5.103 \pm 1.550$	×	$1.775 \pm 0.041$	$1.703 \pm 0.021$	-	$-2.124 \pm 0.102$	$1.256 \pm 0.208$	0.173
Ro	$0.589 \pm 0.133$	$0.466 \pm 0.018$	×	$-0.095 \pm 0.033$	×	×	×	0.184
Ro	$1.103 \pm 0.094$	$0.433 \pm 0.006$	×	-	$-0.137 \pm 0.015$	-	×	0.100
Rm	$1.535 \pm 0.371$	×	$0.749 \pm 0.036$	$-0.264 \pm 0.020$	$0.843 \pm 0.030$	$-0.656 \pm 0.035$	×	0.147
Rm	$2.421 \pm 0.547$	×	$0.757 \pm 0.029$	$-0.257 \pm 0.016$	$0.857 \pm 0.024$	$-0.901 \pm 0.070$	$0.528 \pm 0.139$	0.108

Table 2: Optimal scaling laws obtained by the multiple linear regression method, for  $\text{Ra}_c$ ,  $\text{Ra}_Q^*$  (relation (32) and relation given in the footnote 2), Ro (relation (36) and relation given in the footnote 3) and Rm (relation given in the footnote 4 and relation (38)) (95% confidence intervals). Crosses indicate that the corresponding parameter is chosen not to enter the fit. The dashes indicate that the contribution of the corresponding parameter has been found negligible.

	Pre-factor	$\text{Rm} - \text{Rm}_d$	$\tilde{R} - \tilde{R}_d$	E	Pm	Pr	$\chi_{\text{rel}}$
$\Lambda$	$10.243 \pm 8.619$	$1.091 \pm 0.157$	×	$0.516 \pm 0.132$	×	×	0.698
$\Lambda$	$0.305 \pm 0.212$	$0.879 \pm 0.087$	×	$0.119 \pm 0.101$	$0.787 \pm 0.141$	$-0.820 \pm 0.174$	0.301
$\Lambda$	$0.351 \pm 0.210$	×	$0.796 \pm 0.062$	$-0.072 \pm 0.071$	$1.490 \pm 0.096$	$-1.491 \pm 0.144$	0.233

Table 3: Optimal scaling laws obtained by the multiple linear regression method, for  $\Lambda$  as a function of  $(\text{Rm} - \text{Rm}_d)$  (relation (30) and relation given in footnote 1) and  $(\tilde{R} - \tilde{R}_d)$  (relation (40)) (95% confidence intervals).

Combining (34) and (27) leads to the Viscous-Archimedean-Coriolis (VAC) scaling proposed by King & Buffett (2013)

$$\text{Ro} \sim \text{Ra}_Q^{*1/2} \text{E}^{-1/6}. \quad (35)$$

Its application to the 102 dynamos database is represented in figure 13.a, with a relative misfit  $\chi_{\text{rel}} = 0.201$ . It can be compared to the inertial Ro-scalings  $\text{Ro} \sim \text{Ra}_Q^{*2/5}$  (derived from the IAC balance, see Aubert et al., 2001; Jones, 2011) and  $\text{Ro} \sim \text{Ra}_Q^{*1/3}$  (resulting from mixing length theory, see Christensen, 2010) (see figure 13.b). These three scaling laws provide descriptions of the database of comparable quality. The scaling law (27) for the length scale  $\tilde{\ell}_u^*$  however indicates that the VAC scaling (35) is more relevant to the present study than inertial scaling laws.

The direct multiple linear approach provides the following optimal scaling law expressing Ro as a function of  $\text{Ra}_Q^*$  and E (95% confidence intervals given in table 2) <sup>3</sup> :

$$\text{Ro} \simeq 0.59 \text{Ra}_Q^{*0.47} \text{E}^{-0.10}, \quad \text{with} \quad \chi_{\text{rel}} = 0.184. \quad (36)$$

Replacing the parameter  $\text{Ra}_Q^*$  by its expression (31) in equation (35) yields

$$\text{Rm} \sim (\tilde{R} - 1) \text{E}^{-1/3} \text{Pm} \text{Pr}^{-1} \left( \frac{\text{Pr}}{1 + \text{Pr}} \right)^{2/3}. \quad (37)$$

This relation is essential in order to establish a predictive scaling law for the magnetic field strength, whereas relations (31) and (35) are only intermediate steps in the reasoning. Besides, the dependence of Rm on  $\text{E}^{-1/3}$  counterbalances the dependence of  $\Lambda$  on  $\text{E}^{1/3}$  in (28), and thus removes the dependence of  $\Lambda$  on viscosity in its predictive form. The scaling law (37) applied to the 102 dynamos database is represented in figure 14, with a relative misfit  $\chi_{\text{rel}} = 0.253$ . The role of both terms  $\text{Pr}^{-1}$

<sup>3</sup> A direct numerical fit for Ro as a function of  $\text{Ra}_Q^*$ , E, Pm and Pr yields  $\text{Ro} \simeq 1.10 \text{Ra}_Q^{*0.43} \text{Pm}^{-0.14}$ , with  $\chi_{\text{rel}} = 0.100$  (95% confidence intervals given in table 2). The role of E and Pr are found to be negligible. However the bias in the database (see section 4.2) renders the dependence on Pm unreliable (as E and Pm are correlated in the database).

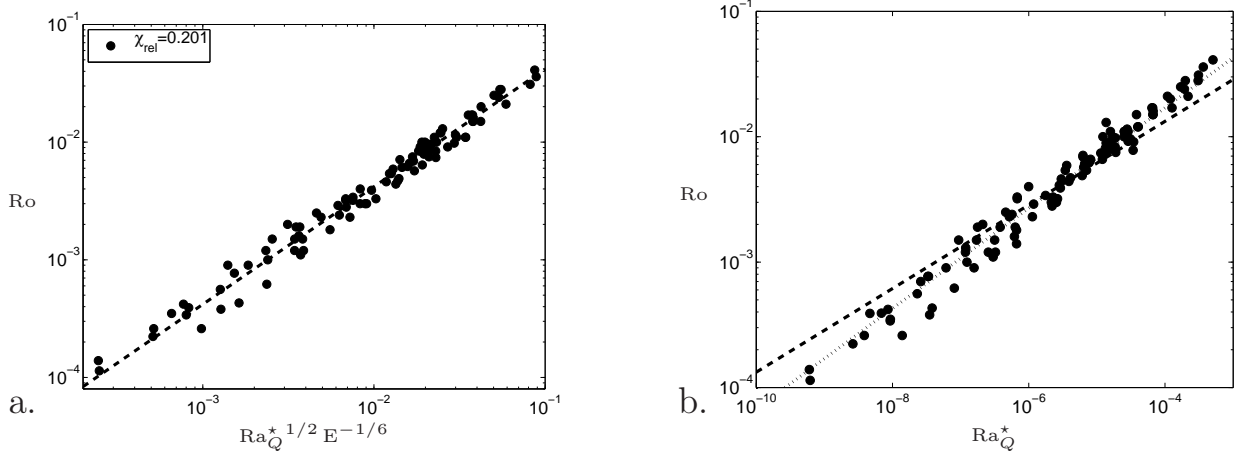


Figure 13: (a) The Rossby number as a function of the flux-based Rayleigh number (a) based on the VAC scaling (relation (35)) (b) on the IAC scaling (dotted line,  $\chi_{\text{rel}} = 0.237$ ) and on the scaling resulting from mixing length theory (dashed line,  $\chi_{\text{rel}} = 0.431$ ). Both graphs rely on the full 102 dynamos database.

and  $(\text{Pr}/(1 + \text{Pr}))^{2/3}$  is illustrated in figure 15: the term  $\text{Pr}/(1 + \text{Pr})^{2/3}$  allows to correct the data corresponding to weak values of  $\text{Pr}$ . The non-negligible dependence on  $\text{Pr}/(1 + \text{Pr})$  is consistent with previous studies of convection which established a dependence of the velocity amplitude on  $\text{Pr}$  more complex than a simple power law dependence (e.g. Schlüter et al., 1965; Tilgner, 1996).

Finally, note that relation (37) can be compared to the optimised fit to the available data. A direct numerical fit provides <sup>4</sup>

$$\text{Rm} \simeq 2.42 \left( \tilde{R} - 1 \right)^{0.76} \text{E}^{-0.26} \text{Pm}^{0.86} \text{Pr}^{-0.90} \left( \frac{\text{Pr}}{1 + \text{Pr}} \right)^{0.53}, \quad \text{with } \chi_{\text{rel}} = 0.108, \quad (38)$$

(the 95% confidence intervals are provided in table 2). The exponents in relations (37) and (38) match to within 20%.

## 4.6 Predictive scaling law for the magnetic field strength

Replacing the flow amplitude in relation (28) by its expression (37) yields the following predictive scaling law

$$\Lambda \sim (\tilde{R} - \tilde{R}_d) \text{Pm} \text{Pr}^{-1} \left( \frac{\text{Pr}}{1 + \text{Pr}} \right)^{2/3}. \quad (39)$$

The direct numerical fit provides in the form of pure power laws

$$\Lambda \simeq 0.35 (\tilde{R} - \tilde{R}_d)^{0.80} \text{E}^{-0.07} \text{Pm}^{1.49} \text{Pr}^{-1.49}, \quad \text{with } \chi_{\text{rel}} = 0.233, \quad (40)$$

(see figure 9.c and table 3 for 95% confidence intervals). The dependence on the Ekman number is here negligible. Besides, we used here the reduced 42 dynamos database for which  $\tilde{R}_d$  can be estimated, the coefficients based on a direct numerical fit are therefore weakly constrained. In particular  $\text{Pr}$  does not vary much in this subsample. Despite of this, the agreement between both expressions is remarkably good, except for a larger exponent of  $\text{Pm}$  for the latter, which remains to be investigated.

<sup>4</sup> Omitting the dependence on  $\text{Pr}/(1 + \text{Pr})$  provides a larger misfit ( $\chi_{\text{rel}} = 0.147$ ) and  $\text{Rm} \simeq 1.54 (\tilde{R} - 1)^{0.75} \text{E}^{-0.26} \text{Pm}^{0.84} \text{Pr}^{-0.66}$  (see figure 9.b and table 2).

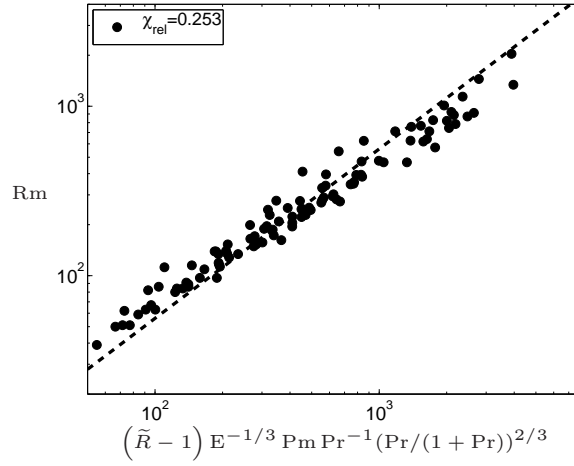


Figure 14: The resulting predictive scaling law for the magnetic Reynolds number as a function of the normalised distance to the onset of convection (relation (37)). This figure relies on the full 102 dynamos database.

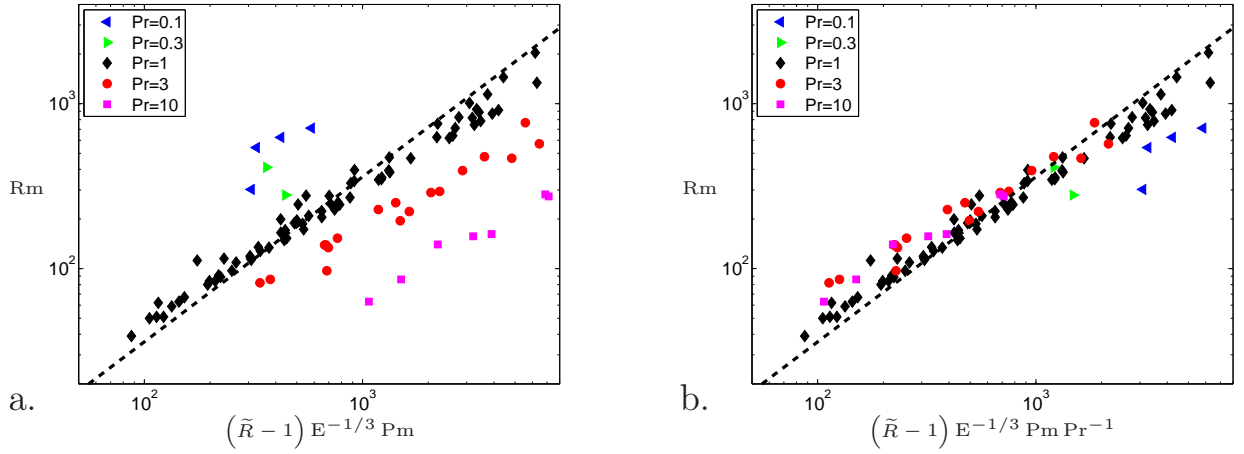


Figure 15: Simplified expressions for  $R_m$  testing the  $Pr$  dependence. The magnetic Reynolds number as a function of the normalised distance to the onset of convection, equation (37) (a) with no correction on  $Pr$  and  $Pr/(1 + Pr)$  (b) with the correction on  $Pr^{-1}$  only. Both graphs rely on the 102 dynamos database.

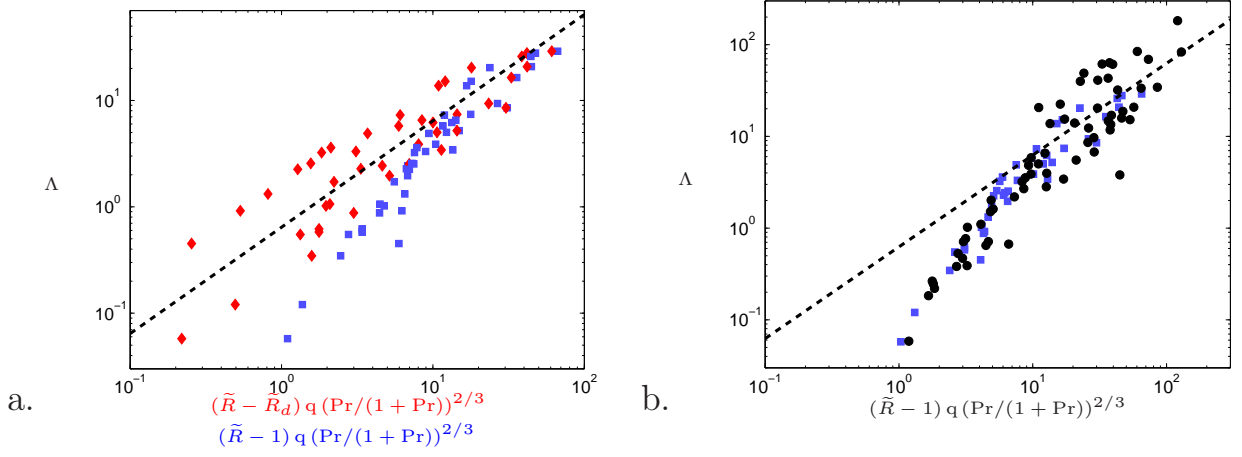


Figure 16: Physically derived predictive scaling law for the magnetic field strength as a function of  $\tilde{R} - \tilde{R}_d$ . (a) Relation (39) (red diamonds), and the same relation but approximating  $\tilde{R}_d$  to unity (blue squares), both applied to the 42 dynamos database. (b) Relation (39) approximating the unknown  $\tilde{R}_d$  contribution to unity, applied to the full (blacks points) and reduced (blue squares) database. The dashed line corresponds to relation (39).

The application of relation (39) to the 42 dynamos database is represented in figure 16.a in red diamonds. The same expression approximating  $\tilde{R}_d$  to unity is plotted using blue squares. As expected, the quality of the approximation decreases with  $\tilde{R}$ . Finally, figure 16.b corresponds to the application of relation (39) to the full database, approximating the unknown  $\tilde{R}_d$  contribution to unity.

Finally, in order to assess the role of the two terms  $\text{Pr}^{-1}$  and  $(\text{Pr}/(1 + \text{Pr}))^{2/3}$  in relation (39), we compare in figure 17 the improvements obtained by each contribution of  $\text{Pr}$ . It highlights the important role of the  $\text{Pr}^{-1}$  term. The role of the  $\text{Pr}/(1 + \text{Pr})$  term in the description of the available numerical database is marginal (compare figures 16.b and 17.b).

Thus, instead of the power based scaling law proposed by Christensen (2010), which can be rewritten as

$$\Lambda \sim f_{\text{ohm}} \text{Ra}_Q^{\star 2/3} \text{E}^{-1} \text{Pm}, \quad \text{with } \chi_{\text{rel}} = 0.452, \quad (41)$$

and which involves measured quantities ( $f_{\text{ohm}}$  and  $\text{Ra}_Q^{\star}$ ), we propose the simple relation (39), which can be reformulated as

$$\Lambda \sim (\tilde{R} - \tilde{R}_d) q \left( \frac{\text{Pr}}{1 + \text{Pr}} \right)^{2/3}, \quad \text{with } \chi_{\text{rel}} = 0.516. \quad (42)$$

The  $\text{Pr}/(1 + \text{Pr})$  dependence comes from the asymptotic expression of the critical Rayleigh number at the onset of convection (24). The moderate variation of  $\text{Pr}$  in the database implies that it can be omitted without significant loss in the quality of the fit (see figure 17.b). This provides an even simpler scaling law, valid for the available range of  $\text{Pr}$

$$\Lambda \sim (\tilde{R} - \tilde{R}_d) q, \quad \text{with } \chi_{\text{rel}} = 0.512. \quad (43)$$

It involves input parameters only, and its derivation was guided by physical arguments. Besides, it is worth noting that (43) as well as (42) imply a dependence of the magnetic field amplitude on the rotation rate  $\Omega$ . This contradicts earlier claims of saturation values independent on the rotation rate.

Relations (41) and (43) are applied to a reduced 33 dynamos database (for which all quantities involved in both relations are available) and represented in figure 18. The relative misfits given in (41), (42), (43) are computed on the basis of this reduced database.

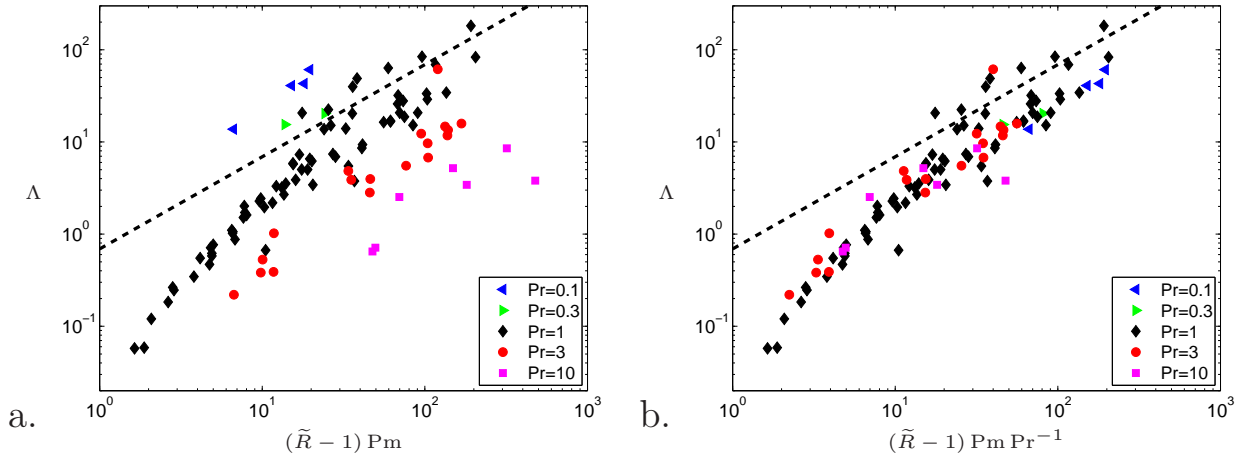


Figure 17: Test of the  $Pr$  dependence in the predictive scaling law (39) applied to the 102 dynamos database approximating the unknown  $\tilde{R}_d$  contribution to unity (a) with no correction on  $Pr$  and  $Pr/(1 + Pr)$  (b) with the correction on  $Pr^{-1}$  only. The dashed line in (a) and (b) corresponds to the scaling law (39).

Note that the power based relation (41) does not involve any distance to the onset of dynamo action. Indeed, the parameter  $Ra_Q^*$  does not vanish at the onset of dynamo action (it vanishes at the onset of convection, see equation (13)). The parameter  $f_{ohm}$  however corrects this issue, as it tends to zero at the onset of dynamo action.

## 5 Conclusion

In this study, we combine a numerical approach, which consists in establishing scaling laws for quantities of interest thanks to a multiple linear regression method applied to numerical data under the approximation of power laws, and a physical approach based either on energetics or on forces balances. Our numerical approach is based on a 102 dynamos database (U. Christensen) corresponding to Boussinesq fully convecting ( $Nu > 2$ ) and dipolar dynamo models.

In a first phase, we focus our attention on scaling laws for the magnetic field strength as a function of the injected power by buoyancy forces, quantified by the flux-based Rayleigh number  $Ra_Q^*$ . We show that the scaling laws previously obtained in the literature mainly correspond to the simple writing of the energy balance between production and dissipation, which is necessarily valid for any dynamo in statistical equilibrium. Such power based scaling laws are thus very general and applicable to any dynamo in statistical equilibrium irrelevantly of the dynamo mechanism (e.g. Schinnerer et al., 2012).

The description of the magnetic dissipation length scale  $\ell_B$  determines the quality of the approximation. Assuming a constant value for  $\ell_B$  already provides a very good description of the numerical database. Improved fits can be obtained based on finer assumptions for  $\ell_B$ . However, none of the proposed scaling laws corresponds to a realistic physically based relation to describe the numerical database (see section 3.4).

The second part of our study aims at establishing predictive scaling laws (i.e. as a function of input parameters only) for the magnetic field strength. Our reasoning is guided by physical arguments such as forces balances, and the numerical database is only used to validate the proposed relations. Indeed, we have shown that scaling laws obtained through a direct numerical fit can be biased by the numerical sample. It is in particular the case for the Ekman and magnetic Prandtl numbers,

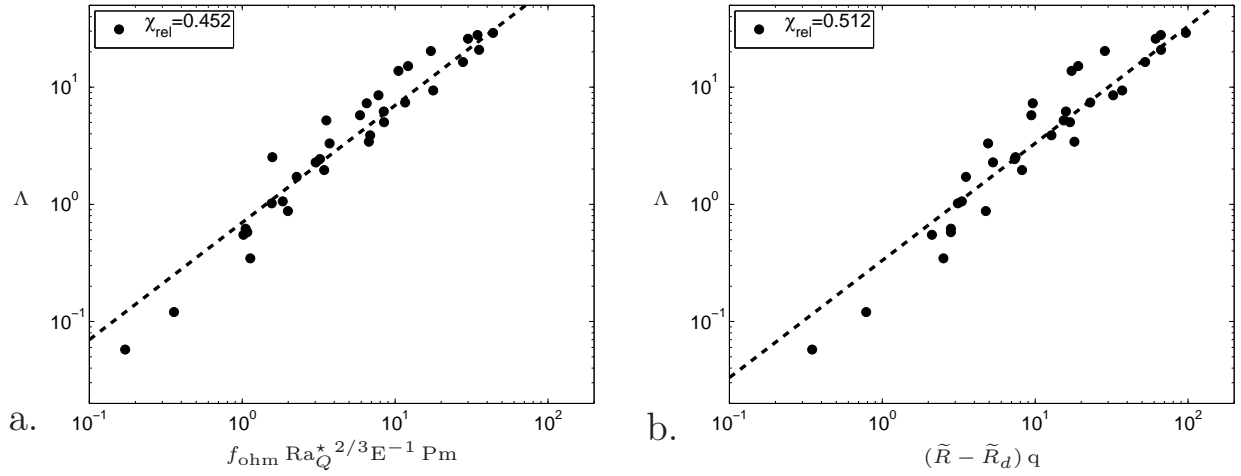


Figure 18: Comparison of the earlier power based scaling law (Christensen, 2010) and our proposed predictive scaling law for the magnetic field strength: relations (a) (41) and (b) (43). Both graphs rely on a reduced 33 dynamos database for which  $\tilde{R}_d$  and  $f_{\text{ohm}}$  are available.

whose ranges are strongly correlated in the database. The flux-based Rayleigh number  $\text{Ra}_Q^*$ , which is a measured quantity, is replaced either by the normalised distance of the Rayleigh number to the onset of convection (denoted as  $\tilde{R} - 1$ ) or by the normalised distance to the onset of dynamo action (measured by  $\tilde{R} - \tilde{R}_d$ ). This last quantity is unfortunately only available for a subset of the numerical database.

Our four control parameters are the Ekman number, the Prandtl number, the magnetic Prandtl number and the relative distance to the onset of convection (resp. dynamo action). Our reasoning follows four steps.

The first step of the reasoning provides a scaling law for the magnetic field strength as a function of the distance to the onset of dynamo in term of flow amplitude, which is  $\Lambda \sim (\text{Rm} - \text{Rm}_d) E^{1/3}$  and which matches numerical data. It is deduced from the balance between the Lorentz force and the viscous force associated to the flow distortion (Fauve & Petrelis, 2007).

The second one consists in establishing the link between the injected power (measured by  $\text{Ra}_Q^*$ ) and  $\tilde{R} - 1$ , by using the definition of  $\text{Ra}_Q^*$ , the relation between  $\text{Nu}$  and  $\tilde{R}$  (e.g. King et al., 2010) and previously established dependences of the critical Rayleigh number at the onset of convection on the Ekman and Prandtl numbers (Busse, 1970).

The third step deals with the derivation of a scaling law for the flow amplitude. The Viscous-Archimedean-Coriolis scaling (King & Buffett, 2013) matches the numerical data. Especially, the characteristic velocity length scale of the flow depends on  $E^{1/3}$  in numerical simulations, which proves that viscous effects play a non-negligible role in the bulk of the flow. The role of inertia is shown to be negligible on this length scale for dipolar dynamos compared to that of viscous effects.

Finally, in a fourth step, the combination of the aforesaid results leads to a surprisingly simple predictive scaling law, that is  $\Lambda \sim (\tilde{R} - \tilde{R}_d) q (\text{Pr}/(1 + \text{Pr}))^{2/3}$ , which involves input parameters only, contrary to previous published scaling laws, and which properly describes available numerical data (as stressed in the text, the  $\text{Pr}$  dependence is not tested by the database and can be omitted here without loss). This scaling law relies on the dominant forces balance in the numerical dynamos. Contrary to power based scaling laws, it is applicable in the parameter range covered by this study, but will not be satisfied in general (e.g. if inertial forces become significant). Besides its predictive power, it also provides information on the underlying forces balance at work in the dynamo simulations.

Introducing predictive scaling laws, based on control parameters only, allows to underline two important ideas. First, the present numerical models do not operate in a dominant forces balance

relevant for the geodynamo. Indeed, viscous effects are shown to be essential and extrapolation to geophysically relevant parameters produces strongly underestimated amplitudes for the magnetic field. Secondly, it allows to demonstrate the clear dependence of the magnetic field strength on the rotation rate  $\Omega$ .

## A The multiple linear regression approach

As in previous studies (Christensen & Tilgner, 2004; Christensen & Aubert, 2006; Stelzer & Jackson, 2013), we restrict our scaling analysis to power laws of the form

$$\mathbf{Y} \propto \alpha \prod_{j=1}^p \mathbf{X}_j^{\beta_j}, \quad (44)$$

where  $\mathbf{Y}$  is the  $n$ -dimensional vector of output data which we want to fit, and  $\mathbf{X}_j$  are the  $p$   $n$ -dimensional predictor variables. Taking the logarithm of (44) transforms the model in a multiple linear regression problem

$$\log(\mathbf{Y}) = \beta_0 + \beta_1 \log(\mathbf{X}_1) + \beta_2 \log(\mathbf{X}_2) + \dots + \beta_p \log(\mathbf{X}_p) + \boldsymbol{\varepsilon}. \quad (45)$$

in which  $\beta_0 = \log(\alpha)$ , and  $\boldsymbol{\varepsilon}$  is an  $n$ -dimensional vector measuring the misfit.

In the following,  $\log(\mathbf{Y})$  is replaced by  $\tilde{\mathbf{Y}}$  and  $\log(\mathbf{X}_j)$  by  $\tilde{\mathbf{X}}_j$  for clarity. The system of  $n$  equations (45) can be represented in matrix notation as

$$\tilde{\mathbf{Y}} = \tilde{\mathbf{X}} \boldsymbol{\beta} + \boldsymbol{\varepsilon}, \quad (46)$$

where  $\tilde{\mathbf{X}}$  is referred to as the design matrix  $[\mathbf{I} \ \tilde{\mathbf{X}}_1 \ \dots \ \tilde{\mathbf{X}}_p]$  and  $\boldsymbol{\beta}$  is a  $(p+1)$ -dimensional vector containing the whole set of regression coefficients. The vector  $\boldsymbol{\beta}$  can be estimated using least square estimates. The misfit  $\boldsymbol{\varepsilon}$  is assumed to follow a Gaussian centered distribution with a variance  $\sigma$  which is assumed to be a constant. The corresponding fitted model is

$$\hat{\tilde{\mathbf{Y}}} = \tilde{\mathbf{X}} \hat{\boldsymbol{\beta}}, \quad (47)$$

where

$$\hat{\boldsymbol{\beta}} = \left( \tilde{\mathbf{X}}^t \cdot \tilde{\mathbf{X}} \right)^{-1} \cdot \tilde{\mathbf{X}}^t \cdot \tilde{\mathbf{Y}}. \quad (48)$$

The variance  $\sigma$  can be estimated by the unbiased estimator  $\hat{\sigma}$  defined as

$$\hat{\sigma}^2 = \frac{1}{n-p-1} \|\hat{\boldsymbol{\varepsilon}}\|^2, \quad \text{where} \quad \hat{\boldsymbol{\varepsilon}} = \mathbf{Y} - \hat{\tilde{\mathbf{Y}}}. \quad (49)$$

As a measure of misfit between data and fitted values, we use as in Christensen & Aubert (2006) the mean relative misfit to the original data  $y_i$  ( $i \in (1, n)$ ), defined as

$$\chi_{\text{rel}} = \sqrt{\frac{1}{n} \sum_{i=1}^n \left( \frac{y_i - \hat{y}_i}{y_i} \right)^2}. \quad (50)$$

The estimator  $\hat{\boldsymbol{\beta}}$  is unbiased and its covariance matrix can be estimated by

$$\hat{\boldsymbol{\sigma}}_{\hat{\boldsymbol{\beta}}}^2 = \hat{\sigma}^2 \left( \tilde{\mathbf{X}}^t \cdot \tilde{\mathbf{X}} \right)^{-1}, \quad (51)$$

which is a  $(p+1) \times (p+1)$  matrix. An estimation of the variance  $\hat{\sigma}_{\hat{\beta}_j}$  of the  $\hat{\beta}_j$  exponent ( $j \in (0, p)$ ) is

$$\hat{\sigma}_{\hat{\beta}_j} = \hat{\sigma} \sqrt{\left( \left( \tilde{\mathbf{X}}^t \cdot \tilde{\mathbf{X}} \right)^{-1} \right)_{jj}}, \quad (52)$$



and the estimator  $(\hat{\beta}_j - \beta_j)/\hat{\sigma}_{\hat{\beta}_j}$  follows a Student distribution (Student, 1908; Fisher, 1925) with  $(n - p - 1)$  degrees of freedom. For the analysis performed in this article,  $(n - p - 1) \approx 100$ . In that case, the coefficient  $\beta_j$  is comprised in the 95% confidence interval

$$\beta_j = \hat{\beta}_j \pm 2 \hat{\sigma}_{\hat{\beta}_j}. \quad (53)$$

This method provides the following power law for  $y$

$$y = \exp(\hat{\beta}_0 \pm 2 \hat{\sigma}_{\hat{\beta}_0}) \prod_{j=1}^p x_j^{\hat{\beta}_j \pm 2 \hat{\sigma}_{\hat{\beta}_j}}, \quad (54)$$

which can be rewritten as

$$y = \left( \exp(\hat{\beta}_0) \cosh(2 \hat{\sigma}_{\hat{\beta}_0}) \pm \exp(\hat{\beta}_0) \sinh(2 \hat{\sigma}_{\hat{\beta}_0}) \right) \prod_{j=1}^p x_j^{\hat{\beta}_j \pm 2 \hat{\sigma}_{\hat{\beta}_j}}. \quad (55)$$

In the present paper, the confidence intervals are provided in separated tables.

In a geometric interpretation where the essential quantity is reported in ordinate and the optimal combination of fitting parameters in abscissa, the mean relative misfit  $\chi_{\text{rel}}$  measures the relative ordinate distance between observations and estimations, without taking the abscissa distance into account. That is why its use is restricted to comparisons of fits for the same quantity  $y$ . Besides, the mean relative misfit  $\chi_{\text{rel}}$  is obviously expected to decrease with the number  $p$  of predictor variables. As the system of equations (1-3) is governed by four non-dimensional parameters (Ra, E, Pm and Pr), the maximum number  $p_{\text{max}}$  of independent predictor variables is equal to 4. For further discussions on fitting errors, we refer the reader to Stelzer & Jackson (2013).

## B Role of the fraction of ohmic dissipation $f_{\text{ohm}}$ in empirical scaling laws for the magnetic field strength

We stress here the pitfalls of direct numerical fits, free from physical insight, by showing that different a priori hypothesis on  $f_{\text{ohm}}$  yield contradictory results.

### B.1 Power based scaling laws derived from multiple linear regressions

As noted in section 3.1,  $f_{\text{ohm}}$  is not at all a trivial parameter, as it involves both controlled and measured quantities. Indeed with our notations, equation (5) can be rewritten as

$$f_{\text{ohm}} = \left( 1 + \frac{\text{Ro}^2}{\text{Lo}^2} \frac{\ell_B^{\star 2}}{\ell_u^{\star 2}} \text{Pm} \right)^{-1}, \quad (56)$$

where we introduced a kinematic dissipation length scale  $\ell_u$  ( $\ell_u^{\star} = \ell_u/L$ ), defined using time averaged quantities as

$$\ell_u^2 \equiv \frac{\int_V \mathbf{u}^2 dV}{\int_V (\nabla \times \mathbf{u})^2 dV} = 2\nu \frac{E_{\text{kin}}}{D_\nu}. \quad (57)$$

The main distinction between the scaling laws (18) and (23) respectively proposed by Christensen & Aubert (2006) and Davidson (2013) relies on the different exponent of  $f_{\text{ohm}}$ .

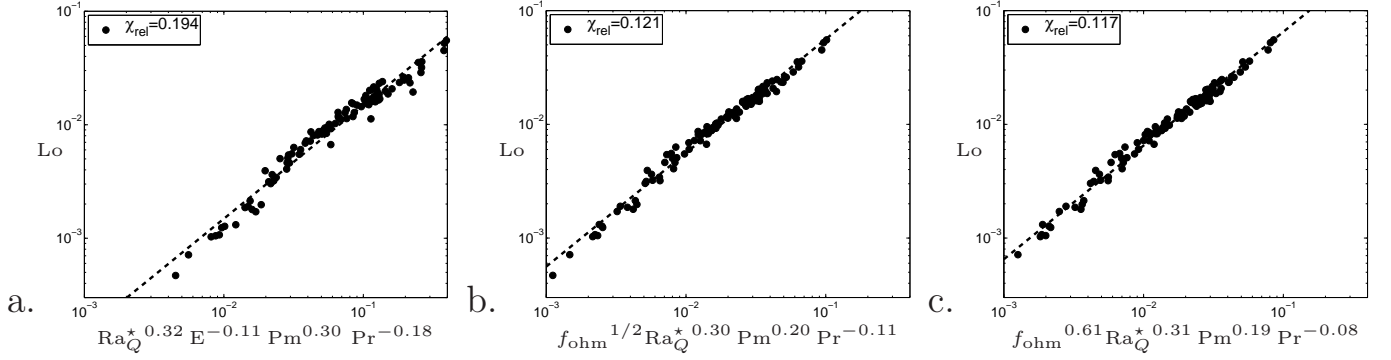


Figure 19: The Lorentz number versus a combination of flux-based Rayleigh number, Ekman number, Prandtl number, magnetic Prandtl number (a) with no  $f_{\text{ohm}}$  dependence (equation (58)), (b) with an additional fixed  $f_{\text{ohm}}^{1/2}$  factor (equation (61)) and (c) an additional  $f_{\text{ohm}}$  dependence with an optimised exponent (equation (62)). This figure relies on the 102 dynamos database.

First considering the best empirical scaling law for the magnetic field strength in our database, ignoring the  $f_{\text{ohm}}$  parameter, we get

$$\text{Lo} \simeq 0.16 \text{Ra}_Q^{*0.32} \text{E}^{-0.11} \text{Pm}^{0.30} \text{Pr}^{-0.18}, \quad \text{with } \chi_{\text{rel}} = 0.194, \quad (58)$$

(see figure 19.a). Note that in the above expression, the right-hand-side vanishes at the onset of convection and not at the onset of dynamo action. This expression is therefore obviously not valid close to the onset of dynamo action.

The balance between energy production and dissipation provides an exponent  $1/2$  for  $f_{\text{ohm}}$  (see section 3.1). The best power law approximation for  $\text{Lo}$  as a function of  $\text{Ra}_Q^*$  obtained by setting the exponent of  $f_{\text{ohm}}$  to  $1/2$  is then

$$\text{Lo} \simeq 0.78 f_{\text{ohm}}^{1/2} \text{Ra}_Q^{*0.32}, \quad \text{with } \chi_{\text{rel}} = 0.256, \quad (59)$$

whereas allowing for a dependence on  $\text{Pm}$  leads to

$$\text{Lo} \simeq 0.64 f_{\text{ohm}}^{1/2} \text{Ra}_Q^{*0.31} \text{Pm}^{0.17}, \quad \text{with } \chi_{\text{rel}} = 0.141. \quad (60)$$

These two expressions correspond to the fits (18) and (19) of Christensen & Aubert (2006). The exponents do not exactly match because the numerical database used here is somewhat larger. However, the two latter relations are rigorously recovered if we apply our algorithm to the 65 dynamos numerical database of Christensen & Aubert (2006). This validates the multiple linear regression approach used in the present paper. The role of the parameter  $\text{Pr}$  is found to be negligible using the 65 dynamos numerical database of Christensen & Aubert (2006). But the 102 dynamos database used here contains more simulations corresponding to  $\text{Pr} \neq 1$  than the earlier Christensen & Aubert (2006) database (32 versus 17). Considering an additional dependence on  $\text{Pr}$  yields

$$\text{Lo} \simeq 0.56 f_{\text{ohm}}^{1/2} \text{Ra}_Q^{*0.30} \text{Pm}^{0.20} \text{Pr}^{-0.11}, \quad \text{with } \chi_{\text{rel}} = 0.121, \quad (61)$$

(see figure 19.b), where the dependence on  $\text{Pr}$  is not negligible. On the contrary, the contribution of the Ekman number appears negligible (taking  $\text{E}$  into account only provides a very minor improvement of  $\chi_{\text{rel}}$  and a small power of  $\text{E}$ ).

It is however natural in a fitting approach to let the exponent  $f_{\text{ohm}}$  be determined by the multiple linear regression approach. Moreover, as noted above, the  $f_{\text{ohm}}$  parameter is usually argued to be equal to unity in planetary dynamos. The best power law with the above parameters is

$$\text{Lo} \simeq 0.66 f_{\text{ohm}}^{0.61} \text{Ra}_Q^{*0.31} \text{Pm}^{0.19} \text{Pr}^{-0.08}, \quad \text{with } \chi_{\text{rel}} = 0.117, \quad (62)$$

	Pre-factor	$f_{\text{ohm}}$	$\text{Ra}_Q^*$	E	Pm	Pr	$\chi_{\text{rel}}$
Lo	$0.157 \pm 0.050$	$\times$	$0.318 \pm 0.027$	$-0.111 \pm 0.053$	$0.295 \pm 0.039$	$-0.176 \pm 0.056$	0.194
Lo	$0.777 \pm 0.168$	$1/2$	$0.322 \pm 0.017$	$\times$	$\times$	$\times$	0.256
Lo	$0.638 \pm 0.080$	$1/2$	$0.313 \pm 0.009$	$\times$	$0.167 \pm 0.023$	$\times$	0.141
Lo	$0.561 \pm 0.063$	$1/2$	$0.302 \pm 0.009$	-	$0.197 \pm 0.021$	$-0.106 \pm 0.033$	0.121
Lo	$0.661 \pm 0.114$	$0.605 \pm 0.091$	$0.309 \pm 0.010$	-	$0.186 \pm 0.023$	$-0.080 \pm 0.039$	0.117
$f_{\text{ohm}}$	$0.073 \pm 0.026$	$\times$	-	$-0.170 \pm 0.030$	$0.180 \pm 0.042$	$-0.178 \pm 0.054$	0.249

Table 4: Optimal scaling laws obtained by the multiple linear regression method, for Lo and  $f_{\text{ohm}}$  (95% confidence intervals): relations (58), (59), (60), (61), (62) and (63).

(see figure 19.c). The contribution of E is negligible, this last relation thus involves five non-dimensional parameters only, which corresponds to the maximum number of independent parameters in the problem (see appendix A). Table 4 gathers the fitted values corresponding to equations (58), (59), (60), (61) and (62) including their 95% confidence interval. The exponents in relation (62) are not significantly different from those in relation (61). In particular, the 95% confidence interval associated to the optimised value 0.61 of the exponent of  $f_{\text{ohm}}$  in (62) includes the value 1/2 provided by the energy balance.

The relative error on the exponents of  $\text{Ra}_Q^*$ , Pm and  $f_{\text{ohm}}$  is in general moderate (less than 15%). The error for the estimation of the exponent of Pr is more important (between 30% and 50%): the distribution of the control parameter Pr in our dataset, although wider than in the dataset used in Christensen & Aubert (2006), is indeed not wide enough to establish a clear dependence on Pr. The parameter E appears only in relation (58) where the output parameter  $f_{\text{ohm}}$  is not taken into account, with a relative error of 50% for the corresponding exponent.

Finally, note that equations (58), (61) and (62) can be related by introducing the best power law approximation for  $f_{\text{ohm}}$  as a function of  $\text{Ra}_Q^*$ , E, Pm and Pr, i.e.

$$f_{\text{ohm}} \simeq 0.07 E^{-0.17} \text{Pm}^{0.18} \text{Pr}^{-0.18}, \quad \text{with } \chi_{\text{rel}} = 0.249, \quad (63)$$

where the contribution of  $\text{Ra}_Q^*$  is found to be negligible (95% confidence intervals in table 4). The high corresponding relative misfit (25%) reveals that the dependence of  $f_{\text{ohm}}$  on other parameters can not be reliably approximated by a simple power law.

## B.2 Extrapolation to natural dynamos

The results of appendix B.1 deserve careful analysis. Equation (62) may be indeed viewed as a minor improvement in the quality of the fit, resulting from the introduction of an additional degree of freedom in the problem. Besides, the  $f_{\text{ohm}}$  parameter involves most of the quantities we are trying to fit, that is to say Lo, Ro,  $\ell_B^*$  and  $\ell_u^*$  (see equation (56)).

Nevertheless, the above study clearly indicates that different scaling laws can be proposed for Lo, depending on exponents considered for  $f_{\text{ohm}}$ . If one adopts the usual assumption that  $f_{\text{ohm}} = 1$  for planetary applications, the resulting relation for such applications will not depend on the exponent of  $f_{\text{ohm}}$ . To illustrate this, we can write equations (58), (61) and (62) in dimensional form assuming  $f_{\text{ohm}} = 1$ . These are respectively

$$B \sim \mu^{1/2} P^{0.32} \Omega^{0.16} L^{-0.37} \rho^{0.18} \nu^{0.01} \eta^{-0.30} \kappa^{0.18}, \quad \text{with } \chi_{\text{rel}} = 0.194, \quad (64)$$

$$B \sim \mu^{1/2} P^{0.30} \Omega^{0.09} L^{-0.51} \rho^{0.20} \nu^{0.09} \eta^{-0.20} \kappa^{0.11}, \quad \text{with } \chi_{\text{rel}} = 0.121, \quad (65)$$

and

$$B \sim \mu^{1/2} P^{0.31} \Omega^{0.07} L^{-0.55} \rho^{0.19} \nu^{0.11} \eta^{-0.19} \kappa^{0.08}, \quad \text{with } \chi_{\text{rel}} = 0.117. \quad (66)$$

	P	$\Omega$	$L$	$\rho$	$\nu$	$\eta$	$\kappa$	$\chi_{\text{rel}}$
$B/\mu^{1/2}$	$0.318 \pm 0.027$	$0.157 \pm 0.134$	$-0.368 \pm 0.241$	$0.182 \pm 0.027$	$0.008 \pm 0.142$	$-0.295 \pm 0.039$	$0.176 \pm 0.056$	0.194
$B/\mu^{1/2}$	$0.302 \pm 0.009$	$0.094 \pm 0.027$	$-0.510 \pm 0.045$	$0.198 \pm 0.009$	$0.091 \pm 0.054$	$-0.197 \pm 0.021$	$0.106 \pm 0.033$	0.121
$B/\mu^{1/2}$	$0.309 \pm 0.010$	$0.073 \pm 0.030$	$-0.545 \pm 0.050$	$0.191 \pm 0.010$	$0.106 \pm 0.062$	$-0.186 \pm 0.023$	$0.080 \pm 0.039$	0.117

Table 5: 95% confidence intervals associated to exponents in the dimensional scaling laws for the magnetic field strength corresponding to relations (64), (65) and (66).

Table 5 gathers the above fitted values and the corresponding confidence intervals. The latter are calculated using the 95% confidence intervals found in the non-dimensional scaling laws, considering their more pessimistic combination. By this process, the three relations can not be distinguished: for the exponents of all parameters, there exists an interval common to the three expressions. But if we consider 70% confidence intervals as Stelzer & Jackson did, the incertitude of the exponent  $\hat{\beta}_j$  is equal to  $\hat{\sigma}_{\hat{\beta}_j}$  instead of  $2\hat{\sigma}_{\hat{\beta}_j}$  (see appendix A). We can also deduce that expression (64) predicts a dependence of B on  $\Omega$  which is twice that of (66). A similar effect can be noted for the dependence on  $\kappa$ . The dependence on  $\eta$  predicted by (64) is also 1.5 higher than that predicted by the scaling law (66). Finally, (64) predicts a much weaker dependence on  $\nu$  than (66) ( $1/10^{\text{th}}$  factor). Thus, in the limit of 70% confidence intervals, the dependence of the magnetic field strength on physical parameters seems to depend on the role given to  $f_{\text{ohm}}$  in the numerical fit.

Using an estimate for the Earth’s core of  $\text{Ra}_Q^* \text{Earth} = 10^{-14}$  (e.g. Christensen & Aubert, 2006) in (58), (61) and (62) yields  $B_{\text{Earth}} = 0.10 \text{ mT}$ ,  $B_{\text{Earth}} = 0.05 \text{ mT}$  and  $B_{\text{Earth}} = 0.05 \text{ mT}$  respectively. It should be compared to the rms magnetic field strength inside the Earth’s core, estimated to be of the order of  $2 - 4 \text{ mT}$  (e.g. see Buffett, 2010; Gillet et al., 2010). Our values above are lower than this estimated value by a factor 20-40, just as the values obtained by Christensen & Aubert (2006) and Stelzer & Jackson (2013).

## C The magnetic dissipation length scale $\ell_B$

### C.1 The $\ell_B$ length scale as a function of the flow amplitude

We interpret here earlier scaling laws in terms of assumptions made on  $\ell_B^*$  and their implications for Ro and  $\ell^*$ .

Christensen & Tilgner (2004) have empirically shown that  $\tau_\eta^* \sim \text{Rm}^{-1}$ . Because  $\tau_\eta^* \sim \ell_B^{*2}$ , this provides  $\ell_B^* \sim \text{Rm}^{-1/2}$  (see figure 20.a, see also Roberts & King, 2013). According to equation (16), this scaling law corresponds to assuming that  $\ell^* \sim 1$ , i.e.  $\ell$  is the width of the spherical shell. It is reasonably consistent with the 102 dynamos database used in this paper, since  $\text{Rm} \ell_B^{*2}$  varies from 0.19 to 1.25, that is to say over about one order of magnitude. Moreover, note that some of the values are higher than unity: it is symptomatic of the role played by correlations between the norm and direction of  $\mathbf{u}$  and  $\mathbf{B}$ . Christensen & Tilgner (2004) have empirically improved the above scaling law to  $\ell_B^* \sim \text{Rm}^{-0.49} \text{Re}^{-0.08}$ , where Re is the Reynolds number ( $\text{Re} = \text{Rm} \text{Pm}^{-1}$ ). This expression can be reformulated as  $\ell_B^* \sim \text{Rm}^{-0.57} \text{Pm}^{0.08}$  (see figure 20.b). Thanks to a larger numerical data sample, this last scaling law has been optimised by Christensen (2010) as  $\ell_B^* \sim \text{Rm}^{-5/12} \text{E}_\eta^{1/12}$  (see figure 20.c), and then by Stelzer & Jackson (2013) as  $\ell_B^* \sim \text{Rm}^{-0.45} \text{E}^{0.05} \text{Pm}^{0.05}$  (see figure 20.d).

As expected, the relative misfit  $\chi_{\text{rel}}$  decreases when the number of predictor variables increases. Moreover, note that fits in figure 20 are based on 102 numerical simulations extracted from the data sample provided by U. Christensen. Thus, the sample used in figure 20 is larger than the one originally used by Christensen & Tilgner (2004) and Christensen (2010), and slightly different from that used by Stelzer & Jackson (2013) (also based on the 185 dynamos database of U. Christensen but including  $f_{\text{dip}} > 0.35$  dynamos).

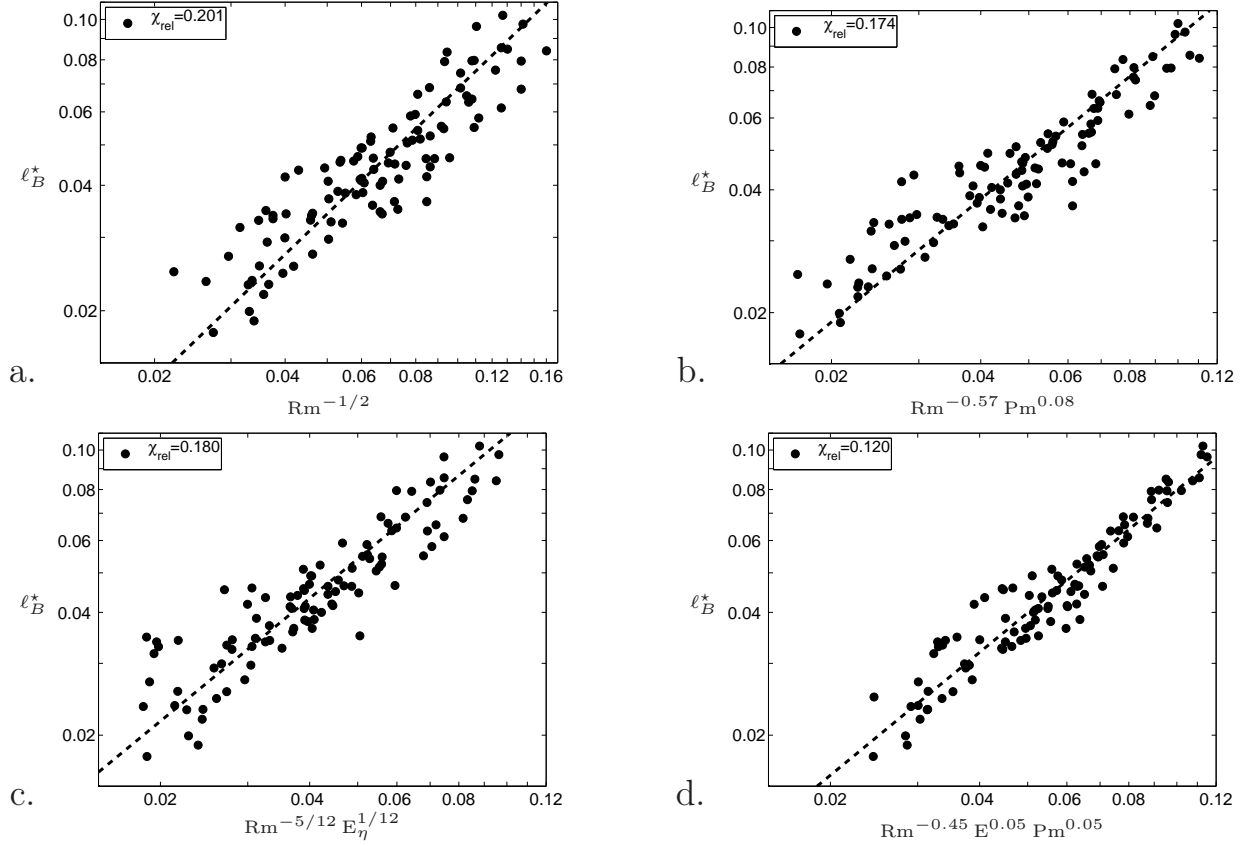


Figure 20: The magnetic dissipation length scale versus a combination of the magnetic Reynolds number, the Ekman number and the magnetic Prandtl number: (a)  $\ell_B^* \sim \text{Rm}^{-1/2}$  (b)  $\ell_B^* \sim \text{Rm}^{-0.57} \text{Pm}^{0.08}$  (both derived from Christensen & Tilgner, 2004) (c)  $\ell_B^* \sim \text{Rm}^{-5/12} \text{E}_\eta^{1/12}$  (Christensen, 2010) (d)  $\ell_B^* \sim \text{Rm}^{-0.45} \text{E}^{0.05} \text{Pm}^{0.05}$  (Stelzer & Jackson, 2013). These graphs rely on the full 102 dynamos database.

Finally, whereas the simple scaling law used in figure 20.a corresponds to a simple physical assumption on the length scale  $\ell$ , the three other laws, albeit more accurate, are simply based on empirical fits.

## C.2 The $\ell_B$ length scale as a function of the injected power

Whereas the four aforesaid scaling laws rely on the magnetic Reynolds number, scaling laws for the magnetic field amplitude based on a production/dissipation balance rely on the flux-based Rayleigh number  $\text{Ra}_Q^*$  (see sections 3.1-3.2). It is therefore natural to seek for relations between the dissipation length scale  $\ell_B^*$  and  $\text{Ra}_Q^*$ .

Indeed, published scaling laws for the amplitude of the magnetic field, such as the empirical scaling laws of Christensen & Aubert (2006) (see our equations (18) and (19)), can readily be translated in terms of scaling laws for  $\ell_B^*$ . Thus, using equations (10) and (12), the scaling laws (18) and (19) respectively imply  $\ell_B^* \sim \text{Ra}_Q^{*-0.16} \text{E}_\eta^{1/2}$ , and  $\ell_B^* \sim \text{Ra}_Q^{*-0.18} \text{E}_\eta^{1/2} \text{Pm}^{-0.39}$ . It is interesting to note that in the representations of relations (18) and (19) by Christensen & Aubert (2006), the x-coordinate varies over six orders of magnitude (see figures 2.a,b in the present paper and figures 8-9 in Christensen & Aubert, 2006) while none of the control parameters varies over such a wide range. Thus, figure 3 (i.e. the above two relations) offers a somewhat more challenging representation of the very same expressions (18) and (19) in so far as the axes vary on a smaller range.

The above scaling laws expressing  $\ell_B^*$  as a function of  $\text{Ra}_Q^*$  were deduced from (18) and (19). As  $\ell_B^*$  is related to both  $\ell^*$  and  $\text{Ro}$ , they also imply relations between these two parameters and  $\text{Ra}_Q^*$ . It is through these relations that the first of these scaling laws for the magnetic field strength was originally physically interpreted by Christensen & Aubert (2006), Christensen (2010) and Jones (2011) (see section 3.4).

## D Length scales in Davidson's (2013) demonstration

The magnetic dissipation length scale denoted as  $\ell_B$  in the present paper is referred to as  $\ell_{\min}$  in Davidson (2013). Besides, he carefully introduced two length scales  $\ell_{\parallel}$  and  $\ell_{\perp}$  (the integral length scales parallel and perpendicular to the rotation axis). The length scale  $\ell_{\parallel}$  can be approximated by  $L$ , and the length scale  $\ell_{\perp}$  corresponds to  $\ell_u$  introduced in the present paper in appendix B.1. Davidson (2013) is interested in planetary dynamos, for which  $f_{\text{ohm}} \simeq 1$ . We consider here the question of the applicability of his analytical results to the length scales computed from the numerical database.

Davidson's dimensional analysis leading to relation (21) is based on the assumption that  $\ell_B^2/\eta$  is independent on the rotation rate. This assumption, which was made in the limit relevant to planetary interiors, does not seem to extend to the parameter regime of numerical models. Indeed, using (9), the scaling law (64) for the magnetic field strength implies

$$\frac{\ell_B^2}{\eta} \sim \Omega^{0.314 \pm 0.268}, \quad (67)$$

(95% confidence interval). Admittedly, the relative confidence interval is large, but the non-dependence of  $\ell_B^2/\eta$  on the rotation rate, while sensible in the regime relevant to the geodynamo, is not relevant to the numerical data used here.

Besides, neglecting viscous effects, he considered the balance of the curl of the Coriolis force, the buoyancy force and the Lorentz force (the so-called MAC-balance, i.e. his equation (10)). Its combination with relation (21) provided by his dimensional analysis leads to  $\ell_B^2 \sim \eta u^{-1} \ell_{\perp}$ , which can be rewritten in its non-dimensional form as

$$\ell_{\perp}^* \sim \text{Rm} \ell_B^{*2}. \quad (68)$$

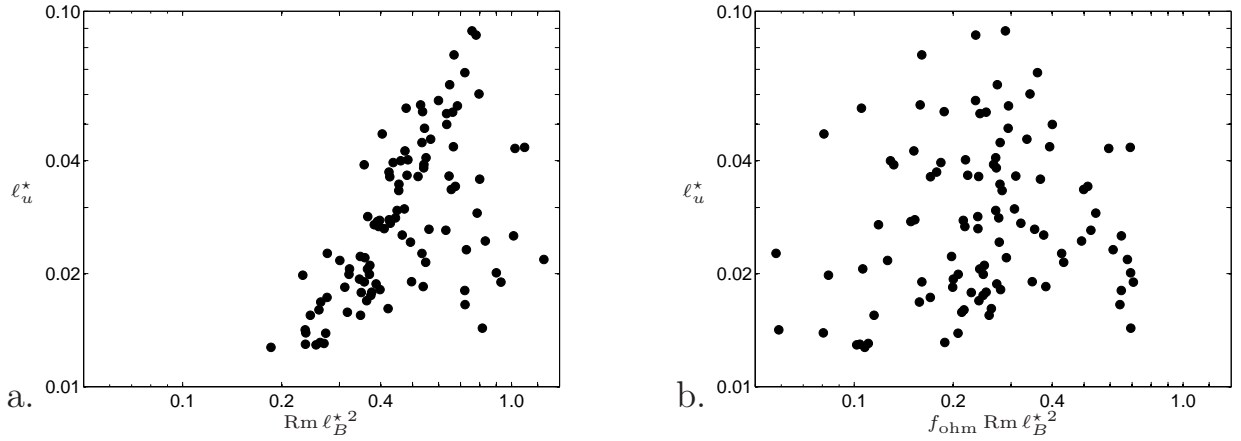


Figure 21: The length scale  $\ell_u^*$  as a function of (a)  $Rm \ell_B^{*2}$  (relation (68)) (b)  $f_{ohm} Rm \ell_B^{*2}$  (relation (69)). These two graphs rely on the 102 dynamos database. This figure highlights that the hypothesis made by Davidson (2013), although well suited for planetary dynamos, are not met by numerical models.

By comparison with equation (16), that means that  $\ell_\perp$  corresponds to our length scale  $\ell$  defined in section 3.3. The distinction between  $\ell$  and  $\ell_\perp$  is proved important in our study. Figure 21.a highlights that they should not be confused. The two assumptions,  $f_{ohm} \simeq 1$  and negligible viscous effects, are indeed not verified in numerical experiments.

If we use equation (22) (equation (9) in Davidson, 2013) rather than (21) (equation (6) in Davidson, 2013) to take  $f_{ohm}$  into account, we get  $\ell_B^2 \sim \eta f_{ohm}^{-1} u^{-1} \ell_\perp$ , which can be rewritten in its non-dimensional form as

$$\ell_\perp^* \sim f_{ohm} Rm \ell_B^{*2}. \quad (69)$$

This expression corresponds to a modified form of relation (68), adapted to  $f_{ohm} < 1$  cases. Figure 21.b shows that even such an  $f_{ohm}$  dependence does not provide a good description of the numerical data. This confirms that the assumption of negligible viscous effects, valid in the bulk of the Earth’s core, is not applicable to present numerical simulations. Davidson’s study therefore relies on assumptions relevant to the geodynamo, but not to present direct numerical simulations.

## E Estimation of the onset of dynamo action

The critical values at the onset of dynamo action  $Ra_d$  gathered in table 1 have been estimated through a linear interpolation of the magnetic energy as a function of the Rayleigh number near the onset of dynamo action (see section 4.1). As underlined by Morin & Dormy (2009), the dynamo bifurcation can be either supercritical or subcritical (or take the form of isola), the nature of the bifurcation depending on the parameters. The estimation of the critical Rayleigh number in the former case is represented in figure 22.a: the linear interpolation of data near the dynamo threshold provides  $Ra_d$ . In the case of subcritical bifurcations, the critical  $Ra_d$  estimated by our method corresponds to the continuation of the subcritical branch, as shown in figure 22.b. A similar approach is used to determine  $Rm_d$ .

## Acknowledgments

The authors want to acknowledge stimulating discussion with Peter Davidson and gratefully thank Uli Christensen for sharing his numerical database.

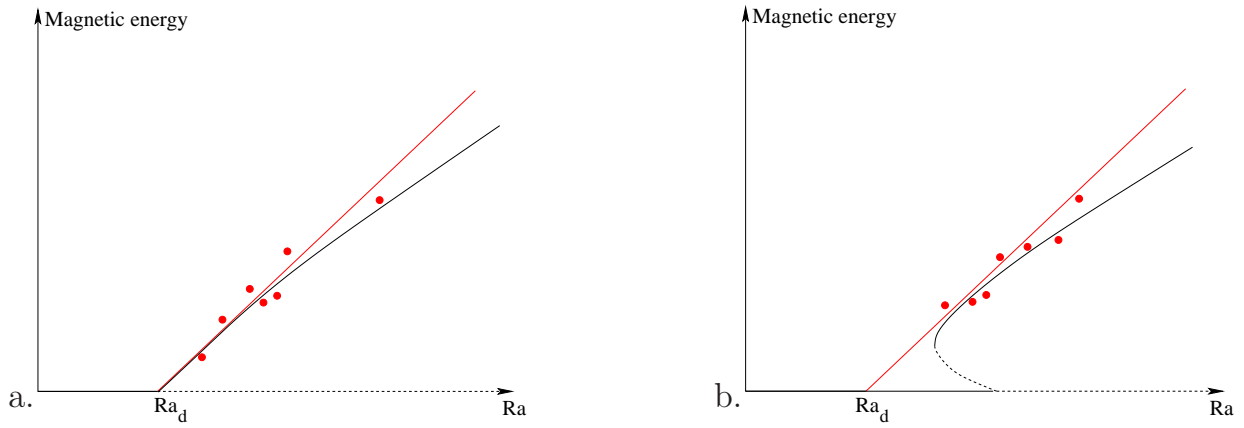


Figure 22: Schematic representation of the behaviour of the magnetic energy as a function of the Rayleigh number, for a (a) supercritical and (b) subcritical dynamo bifurcation. The solid (resp. dashed) lines indicate stable (resp. unstable) branches (see Morin & Dormy, 2009). The linear interpolation (red solid line) associated to data (red points) provides the value of  $Ra_d$  in both cases.

## References

- Aubert, J., H.-C. Nataf, P. Cardin, and J.-P. Masson, 2001 : “A systematic experimental study of rapidly rotating spherical convection in water and liquid gallium.” *Phys. Earth planet. Int.*, 128, 51–74.
- Aurnou, J., 2007 : “Planetary core dynamics and convective heat transfer scaling.” *Geophys. Astrophys. Fluid Dyn.*, 101 (5-6), 327–345.
- Buffett, B.A., 2010 : “Tidal dissipation and the strength of the Earth’s internal magnetic field.” *Nature*, 468(7326), 952–955.
- Busse, F.H., 1970 : “Thermal instabilities in rapidly rotating systems.” *J. Fluid Mech.*, 44 (part 3) : 441–460.
- Carrigan, C.R. and F.H. Busse, 1983 : “An experimental and theoretical investigation of the onset of convection in rotating spherical shells.” *J. Fluid Mech.*, 126, 287–305.
- Chandrasekhar, S., 1961 : *Hydrodynamic and hydromagnetic stability*, Clarendon.
- Christensen, U.R., 2010 : “Dynamo Scaling Laws and Applications to the Planets.” *Space Sci. Rev.*, 152, 565–590.
- and A. Tilgner, 2004 : “Power requirement of the geodynamo from ohmic losses in numerical and laboratory dynamos.” *Nature*, 429, 169–171.
- and J. Aubert, 2006 : “Scaling properties of convection-driven dynamos in rotating spherical shells and application to planetary magnetic fields.” *Geophys. J. Int.*, 166, 97–114.
- , P. Olson, and G.A. Glatzmaier, 1999 : “Numerical modelling of the geodynamo: a systematic parameter study.” *Geophys. J. Int.*, 138, 393–409.
- , V. Holzwarth, and A. Reiners, 2009 : “Energy flux determines magnetic field strength of planets and stars.” *Nature*, 457, 167–169.



- Cornillon, P.-A. and E. Matzner-Lober, 2010 : *Regression avec R*, 3rd ed., Springer.
- Davidson, P.A., 2013 : “Scaling laws for planetary dynamos.” *Geophys. J. Int.*, doi: 10.1093/gji/ggt167.
- Dormy, E., A.M. Soward, C.A. Jones, D. Jault, and P. Cardin, 2004 : “The onset of thermal convection in rotating spheric shells.” *J. Fluid Mech.*, 501, 43–70.
- and J.-L. Le Mouél, 2008 : “Geomagnetism and the dynamo: where do we stand?” *C. R. Physique*, 9, 711–720.
- Fauve, S. and F. Petrelis, 2007 : *Mathematical aspects of natural dynamos*, E. Dormy and A.M. Soward ed., CRC press.
- Fisher, R.A., 1925 : “Applications of Student’s distribution.” *Metron*, 5, 90–104.
- Gillet, N., D. Jault, E. Canet, and A. Fournier, 2010 : “Fast torsional waves and strong magnetic field within the Earth’s core.” *Nature*, 465(7294), 74–77.
- Jones, C.A., 2011 : “Planetary magnetic fields and fluid dynamos.” *Annu. Rev. Fluid Mech.*, 43, 583–614.
- , A.M. Soward, and A.I. Mussa, 2000 : “The onset of thermal convection in a rapidly rotating sphere.” *J. Fluid Mech.*, 405, 157–179.
- King, E.M. and B.A. Buffett, 2013 : “Flow speeds and length scales in geodynamo models: the role of viscosity.” *Earth and Planetary Science Letters*, 371–372, 156–162.
- , K. M. Soderlund, U.R. Christensen, J. Wicht, and J. M. Aurnou, 2010 : “Convective heat transfer in planetary dynamo models.” *Geochem. Geophys. Geosyst.*, 11 (6) : Q06016.
- , S. Stellmach, J. Noir, U. Hansen, and J. M. Aurnou, 2009 : “Boundary layer control of rotating convection systems.” *Nature*, 457 (7227), 301–304.
- Kippenham, R. and A. Weigert, 1990 : *Stellar structure and evolution*, Springer, Berlin.
- Montgomery, D.C., E.A. Peck, and G.G. Vining, 2001 : *Introduction to linear regression analysis*, 3rd ed ed., John Wiley, New-York.
- Morin, V. and E. Dormy, 2009 : “The dynamo bifurcation in rotating spherical shells.” *Int. J. Mod. Phys. B*, 23 (28-29) : 5467–5482.
- Petrelis, F. and S. Fauve, 2001 : “Saturation of the magnetic field above the dynamo threshold.” *Eur. Phys. J. B*, 22, 273–276.
- Roberts, P., 1968 : “On the thermal instability of a rotating-fluid sphere containing heat sources.” *Phil. Trans. A*, 263, 93–117.
- , 1988 : “Future of geodynamo theory.” *Geophys. Astrophys. Fluid Dyn.*, 44, 3–31.
- Roberts, P. H. and E. M. King, 2013 : “On the genesis of the Earth’s magnetism.” *Rep. Prog. Phys.*, 76, 55p.
- Schlüter, A., D. Lortz, and F. Busse, 1965 : “On the stability of steady infinite amplitude convection.” *J. Fluid Mech.*, 23 (part I) : 129–144.

- Schrinner, M., 2012 : “Rotational threshold in global numerical dynamo simulations.” *Mon. Not. R. Astron. Soc.*, 000, 1–6.
- Schrinner, M., L. Petitdemange, and E. Dormy, 2012 : “Dipole Collapse and Dynamo Waves in Global Direct Numerical Simulations.” *Astrophysical Journal*, 752, 121.
- Soderlund, K.M., E.M. King, and J.M. Aurnou, 2012 : “The influence of magnetic fields in planetary dynamo models.” *Earth and Planetary Science Letters*, 333-334, 9–20.
- Stelzer, Z. and A. Jackson, 2013 : “Extracting scaling laws from numerical dynamo models.” *Geophys. J. Int.*, 193, 1265–1276.
- Stevenson, D.J., 1979 : “Turbulent thermal convection in the presence of rotation and a magnetic field: a heuristic theory.” *Astrophys. Fluid Dyn.*, 12, 139–169.
- Student, 1908 : “The probable error of a mean.” *Biometrika*, 6, 1–25.
- Takehiro, S.-I., M. Ishiwatari, K. Nakajima, and Y.-Y. Hayashi, 2002 : “Linear stability of thermal convection in rotating systems with fixed heat flux boundaries.” *Geophys. Astrophys. Fluid Dynamics*, 96 (6) : 439–459.
- Tilgner, A., 1996 : “High-Rayleigh-number convection in spherical shells.” *Phys. Rev. E.*, 53, 4847–4851.
- Zhang, K. and X. Liao, 2004 : “A new asymptotic method for the analysis of convection in a rapidly rotating sphere.” *J. Fluid Mech.*, 518, 319–346.